In presenting this dissertation as a partial fulfillment of the requirements for an advanced degree from the Georgia Institute of Technology, I agree that the Library of the Institution shall make it available for inspection and circulation in accordance with its regulations governing materials of this type. I agree that permission to copy from, or to publish from, this dissertation may be granted by the professor under whose direction it was written, or, in his absence, by the Dean of the Graduate Division when such copying or publication is solely for scholarly purposes and does not involve potential financial gain. It is understood that any copying from, or publication of, this dissertation which involves potential financial gain will not be allowed without written permission.

[redacted]

Gunnar Sigurdsson

DISCHARGE CHARACTERISTICS OF AN EMBANKMENT-SHAPED WEIR

A THESIS

Presented to

the Faculty of the Graduate Division

Georgia Institute of Technology

In Partial Fulfillment

of the Requirements for the Degree

Master of Science in Civil Engineering

By

Gunnar Sigurdsson

June 1955

DISCHARGE CHARACTERISTICS

OF AN EMBANKMENT-SHAPED WEIR

Approved: [redacted]

[redacted]

[redacted]

Date Approved by Chairman: Aug. 19, 1955

ACKNOWLEDGMENTS

The writer is grateful to all those who made this thesis possible. In particular he acknowledges the work of Messrs. R.L. Chapman, C.J. Chi, H.R. Henry and H.Y. Lu, who, in 1947-1949, performed the tests which are designated Series A to D, inclusive. The members of the thesis reading committee were Dr. M.R. Carstens, Prof. G.W. Rainey and Prof. C.E. Kindsvater, under whose guidance this work was performed. Mr. Kindsvater not only suggested the project but gave much valuable time and assistance in its execution. The writer is indebted to Mr. Homer J. Bates, laboratory technician, for assistance in the construction of the experimental facilities.

The research and graduate study culminating in this thesis was sponsored by the American Society of Civil Engineers through its J. Waldo Smith Hydraulic Fellowship. The Fellowship, established in 1938, was made possible with funds bequeathed to the Society by the late J. Waldo Smith, Honorary Member A.S.C.E. Mr. Karl R. Kennison was the chairman of a committee which selected the writer as the recipient of the fellowship for the year 1954-1955.

TABLE OF CONTENTS

LIST OF TABLES

LIST OF FIGURES

ABSTRACT

The flow of water over highway embankments occurs when flood discharges exceed the combined capacities of bridge and culvert waterways. As an overflow structure the embankment is a form of broad-crested weir. Depending on the rate of flow, the roughness of the surface, and the relative height of the tailwater, the discharge over an embankment may be described as "free", "submerged", "plunging", or "surface" flow, the last two being sub-classifications of free flow.

The discharge characteristics of an embankment can be related to the theoretical equation of discharge for broad-crested weirs. Because the conditions assumed for its derivation are never actually satisfied, however, a practical equation involves experimentally determined coefficients. A semi-analytical, free-discharge equation is

$$q = 3.09 \left(1 - \frac{3}{2} \frac{\delta_2^*}{H}\right) H^{3/2} \qquad (19)$$

where (δ_2^*) is the discharge-displacement, boundary-layer thickness at the crown of the roadway. This equation is of general significance only to the extent that (δ_2^*) can be computed for all shapes, sizes and roughnesses of embankments. No general, analytical expression for the influence of tailwater submergence is available.

It was the purpose of this thesis to investigate the discharge characteristics of highway embankments. Emphasis was given to free discharge over smooth-surfaced embankments. Experimental data from two previous investigations were re-analyzed and included with the results of the writer's

experiments on a 1:9-scale model of a typical embankment. Considerable data were collected on the external characteristics of the flow pattern, including the transition phenomena which relate the various flow regimes. Empirical relationships which describe the influence of roughness and tailwater submergence were obtained.

The derivation and experimental substantiation of equation 19 was the principal objective of the writer's investigation. It was necessary, therefore, to review the theoretical considerations involved in the growth of turbulent boundary layers in accelerated flows with convective pressure gradients. The evaluation of (δ_2^*) in equation 19 depends on the experimental determination of certain characteristic parameters in the boundary-layer growth equation. From the results of the writer's experiments it is apparent that additional data pertaining to these parameters is needed (a) to define the magnitude and nature of the influence of the separation zone which forms at the intersection of the upstream embankment and shoulder surfaces, (b) to establish the virtual origin of the boundary-layer, (c) to determine an integrable expression for the convective-acceleration term of the boundary-layer growth equation, and (d) to describe the influence of boundary roughness.

It was established that the convective acceleration over the embankment can be described by a simple analytical expression. It was also determined that, over most of the upstream portion of the top of the embankment, the velocity distribution in the boundary layer can be described by a 1/7-power equation. Whereas data are lacking for establishing the general validity of equation 19, it was remarkably well substantiated for the conditions of the writer's tests.

CHAPTER I

INTRODUCTION

Description of the Problem.--This investigation is concerned with certain aspects of the fluid mechanics of the flow of water over highway embankments. It includes an exploration of theoretical considerations and the results of a limited experimental investigation of a particular form of highway embankment. Among the many aspects of the whole problem which have been excluded, therefore, are the influence of many geometrical variables which characterize both the embankment and the adjacent channel reaches. Detailed consideration of erosion characteristics and their alleviation is also excluded.

The flow of water over highway embankments occurs when flood discharges exceed the combined capacities of bridge and culvert waterways. The hydraulic engineer is interested principally in two problems which result from this occurrence: (1) the determination of the peak flood flow, and (2) the design of measures to protect the embankment from destructive erosion. The solutions for both these problems depend on knowledge of the discharge characteristics of the embankment. Agencies responsible for the collection and compilation of stream flow records, such as the U.S. Geological Survey, have been especially concerned with embankment hydraulics. More recently, however, similar problems have occurred in design offices in connection with new highways located in the extensive swampy areas of the Southeastern states. Here the problem is associated with the economic

question of constructing many miles of roadway to a level which would seldom, if ever, be overtopped--or of building the highway to a level which could be overtopped without excessive damage.

As an overflow structure, the highway embankment is a form of broad-crested weir. The normal range of boundary conditions and flow conditions embraces several regimes of flow. At low heads, boundary-layer influence is dominant. At high heads and "free" discharge, boundary-layer influence is negligible and form effects predominate. For all conditions of free discharge the embankment acts as a control. For the condition of high tailwater and "submerged" discharge, however, the tailwater is the control. The flow pattern in general is characterized by curvilinear, accelerating and decelerating flow, boundary-layer growth under conditions of non-uniform pressure gradient, and non-hydrostatic pressure distribution. It follows, therefore, that a comprehensive analytical solution is impossible.

The Basic Embankment Section.--The basic highway embankment cross-section assumed for this study is shown in figure 1. In this definitive sketch, (P) is the total height of the embankment; (L_s) is the width of the shoulder; (L_r) is the width of the roadway; (S_e) is the slope of the embankment; (S_s) is the slope of the shoulder; and (S_r) is the slope of the roadway. In addition, (e) is the absolute roughness of the embankment surfaces. Such a simplified description of the embankment form is based on the following assumptions: (1) The embankment surface, shoulder surface, and each half of the roadway surface are planes, (2) the cross-section is symmetrical about the vertical centerline, (3) the plane surfaces upstream and downstream from the embankment are horizontal and smooth, and both

surfaces are at the same elevation, and (4) the crown of the roadway is horizontal and perpendicular to the line of flow.

The primary variables required to describe the flow of water over the embankment are shown in figure 2. These include: (h), the piezometric head of the upstream water surface measured with respect to the crown of the roadway; (t), the piezometric head of the downstream water surface with respect to the crown; and (q) the discharge per foot of length of the roadway.

General Analysis of the Problem.--The variables describing the boundary and flow characteristics of the basic embankment section are defined in the preceding section. The fluid properties involved in the discharge function are (γ), the specific weight; (ρ), the density; and (μ), the viscosity of the fluid. An expression which contains all the variables is:

$$f_1 (P, L_s, L_r, S_e, S_s, S_r, e, h, t, q, \gamma, \rho, \mu) = 0. \qquad (1)$$

As there are three independent dimensions and thirteen variables in equation 1, a maximum of ten independent dimensionless ratios can be formed,

$$f_2 \left(\frac{P}{h}, \frac{L_s}{L_r}, S_e, S_s, S_r, \frac{e}{h}, \frac{h}{L_r}, \frac{t}{h}, \frac{\frac{q}{h}}{\sqrt{\frac{\gamma}{\rho} h}}, \frac{q\rho}{\mu} \right) = 0 \qquad (2)$$

Recognizing that the last ratio in equation 2 is a form of the Reynolds number ($\underline{R}$) and that the next to the last ratio is a form of the Euler number or a coefficient of discharge (C), it follows that

$$C \sim q / \sqrt{g} h^{3/2} = f_3 \left(\frac{P}{h}, \frac{L_s}{L_r}, S_e, S_s, S_r, \frac{e}{h}, \frac{h}{L_r}, \frac{t}{h}, \underline{R} \right) \qquad (3)$$

Scope of the Investigation.--For all of the tests summarized in this thesis the shape of the embankment section was held constant. Values of L_s, L_r, S_e, S_s, and S_r shown in figure 1 were based on a design for secondary bituminous-surfaced highways used by the Georgia Highway Department in 1947. For these tests, therefore,

$$C = f_4 \left(\frac{P}{h} , \frac{e}{h} , \frac{h}{L_r} , \frac{t}{h} , \frac{R}{} \right) \qquad (4)$$

For all but one series of tests made by the writer, (P) was also constant. Three values of (e) were included in the tests. It should be observed that, for free-discharge conditions, the ratio (t/h) is insignificant and ($\underline{R}$) is proportional to (q).

The tests completed in 1947-1948 were made in a three-foot-wide flume on a 1:6-scale model of the embankment section. Tests completed in 1949 were made in a 15-inch-wide flume on a 1:12-scale model. Tests made by the writer were performed in the three-foot flume on a 1:9-scale model. In each case the maximum discharge was determined by the capacity of the circulating water system.

Tests made on the 1:6- and 1:12-scale models were largely concerned with the definition of the discharge coefficient for both free-and submerged-flow conditions. Considerable information regarding the shape of the water-surface profile and the definition of the several distinct flow regimes was obtained from these tests. Some data on the effect of roughness and a small amount of data on the velocity distribution over the roadway were also obtained. The results of these tests are described in a subsequent section.

In the writer's experimental program, greater emphasis was given the problem of defining the internal characteristics of the flow pattern. This involved, principally, an investigation of the boundary layer and its influence on free-discharge characteristics. In addition, limited data were obtained on the influence of submergence, roughness, and roadway height, and on the conditions which define the various flow regimes.

Important topics of study which were necessarily omitted because of lack of time included: (1) the influence of the boundary layer along the side walls of the experimental flume, (2) the influence of the boundary layer on the transitional phenomena associated with the different flow regimes, including submerged flow, (3) the influence of major variations in embankment shape, and (4) additional data on the effect of roadway height and roughness.

Review of the Literature.--The only research publication on embankment hydraulics which is known to the writer is a paper by D.L. Yarnell and F.A. Nagler (1). This research was primarily concerned with the flow of water over railway embankments. A limited number of tests was made on flat-topped embankments with the rails removed. The data presented consisted primarily of discharge coefficients for both free and submerged discharge. Scatter in the data indicates questionable accuracy. Internal characteristics of the flow pattern were not investigated.

Because the highway embankment is logically classified as a form of broad-crested weir, the literature in this field also is pertinent to the writer's investigation. The works of Bazin and others have been summarized by Horton (2). Other publications of importance are those by Woodburn (3) and Prentice (4). Most of these papers are concerned

principally with the empirical evaluation of the discharge coefficient. Prentice, however, obtained valuable information on the distribution of velocities and pressures outside the boundary layer.

Ippen (5) suggested a method of correlating model tests on broad-crested weirs by taking into account an estimated boundary-layer thickness on the sides of the flume as well as the surface of the weir. He attempted with partial success to apply his analysis to Woodburn's data.

The most extensive investigation of the discharge characteristics of highway embankments was that performed in the Hydraulics Laboratory of the Georgia Institute of Technology in 1947-1949. As the research for this thesis was largely an outgrowth of the previous investigation, a brief history is given below. A summary of the unpublished results is given in Chapter II.

History of Previous Research at Georgia Tech.--Research at the Georgia Institute of Technology on the hydraulics of highway embankments was begun in November 1947. The original project was initiated when representatives of the Georgia Highway agreed to participate with the Institute in a jointly sponsored investigation under the direction of Professor C.E. Kindsvater. The services of Mr. R.L. Chapman were a major contribution of the Highway Department to the first phase of the work. The tests made by Mr. Chapman (Series A) included water-surface profiles, discharge calibrations, and velocity distributions on a 1:6-scale model of the embankment shape described above. This series of tests was completed in December 1947.

Series B and C tests on a rebuilt version of the 1:6-scale model were begun in April 1948 by graduate students C.J. Chi and H.R. Henry.

These tests were made to check and extend the work performed in Series A. Test Series C was completed by Mr. Chi in July 1948.

In February 1948, Mr. H.Y. Lu, graduate student, began the Series D tests on a 1:12-scale model of the embankment. The purpose of his tests was to determine the effect of model scale and roughness. The work was terminated unfinished in June 1949.

A summary of the results of test Series A to D, inclusive, is contained in the following section.

CHAPTER II

SUMMARY OF PREVIOUS RESEARCH AT THE GEORGIA INSTITUTE OF TECHNOLOGY

Scope of Previous Investigations.--The research discussed in this chapter was performed intermittently in the period 1947 - 1949. The first series of tests, Series A, was intended to define the general characteristics of the flow pattern, with emphasis on the experimental evaluation of the discharge coefficient in the weir equation. Series B and Series C tests were performed to check and extend the results obtained in Series A. All three series were performed on a 1:6-scale model of the basic form described in Chapter I and shown in figure 1. Test Series D was performed on a 1:12-scale model of the same form. These tests, terminated in 1949, were intended to define the effect of model scale and to extend the scope of the previous investigation. Series A and Series B tests included measurements of surface profiles in addition to the measurements pertinent to calibration. A limited number of velocity-distribution measurements were included in the Series A tests.

Description of the 1:6- and 1:12-Scale Models.--The tabulation on figure 1 gives the design suggested in 1947 by the Georgia Highway Department as a typical section for a secondary, bituminous-surfaced highway. The height of the embankment (P) for all tests in Series A to D, inclusive, was 10.5 feet (prototype units). The original 1:6-scale model was built on a framework of wood, covered with masonite (Series A and C) or aluminum (Series B). The 1:12-scale model was built on a metal framework with an

aluminum surface. For Series A and C the surfaces made of tempered masonite were hydraulically rough because they were installed with the checkered side of the masonite exposed. In Series B and D the surfaces were hydraulically smooth because they were made of polished aluminum plate. Figures 3 and 4 show the 1:6- and 1:12-scale models. The masonite surfaces in Series A proved to be very unsatisfactory because of excessive changes in dimensions when wetted. The surfaces became quite irregular, and gages had to be zeroed frequently.

In Series A the discharge was measured with a calibrated sharp-crested weir. In Series B and C a calibrated bend meter was used for the discharge measurements. A bend meter and orifices of four different sizes were employed in Series D. The maximum flow for the 1:6-scale models was 5.1 cubic feet per second in a flume three feet wide (q = 1.7 cubic feet per second per foot). The maximum flow for the 1:12-scale model was 1.8 cubic feet per second in a flume fifteen inches wide (q = 1.4 cubic feet per second per foot). The velocity distribution upstream from the models was irregular, but similar, in both flumes. High-velocity surface currents existed at high discharges.

Surface profiles were determined with a point gage, velocities with a pitot-static tube. Headwater and tailwater levels were measured with hook gages located over stilling wells connected to floor manometers.

A summary of the model characteristics involved in Series A to D, inclusive, is given in table 1.

Table 1. Summary of 1947-1949 Tests

Series	Scale	Surface	Height (P)
A	1:6	rough (masonite)	10.5 ft (prototype)
B	1:6	smooth (aluminum)	"
C	1:6	rough (masonite)	"
D	1:12	smooth (aluminum)	"

Description of the External Flow Patterns.--An important contribution of the 1947-1949 tests was a classification of the different flow patterns which characterize the flow of water over embankments. Doubtless the most important classification is that which divides "free" flow from "submerged" flow. Free flow occurs when the embankment acts as a control section. This condition is associated with low tailwater levels. Submerged flow occurs when the discharge is controlled by the tailwater level. This condition, obviously, is associated with high tailwater levels. The transition point between free and submerged flow has been described as "incipient submergence."

Important sub-classifications of free flow were suggested by the early tests. It is generally recognized that free flow is sometimes characterized by the occurrence of a high-velocity, plunging jet at the downstream side of the embankment. At other times the high-velocity jet occurs on the surface of the tailwater. These "plunging" and "surface" flow patterns are illustrated on figure 5. It is not generally known that the transition from surface flow to plunging flow, and vice versa, occurs within a well-defined range of tailwater levels. Although the tailwater level at which the transition occurs in any one instance is clearly defined, it is critically dependent on the history of the changing flow pattern. In other words, if the flow is initially plunging and the tailwater is low, the plunging flow pattern will persist as the tailwater level rises to an "upper tailwater limit" before changing suddenly to surface flow. On the other hand, if the tailwater is initially high and the high-velocity jet is on the surface of the tailwater, this condition will persist as the tailwater drops to a "lower limit" before changing to plunging

flow. The stability or persistence of the flow patterns within the transition range is related to the inertia of the rollers which occur downstream from the embankment and which are shown on figure 5.

Figures 6 and 7 show complete water-surface profiles for typical tests illustrating the various flow regimes described above. The transition range marking the tailwater level limits within which free discharge can be either plunging flow or surface flow is designated on figure 7 by profiles marked (c) and (d). Figures 8 and 9 include photographs of the changes in the flow pattern near the downstream shoulder during a sequence of rising and falling tailwater levels. Figure 10 shows test data which illustrate the well-defined transition range for plunging and surface flow from Series B and D tests. Figure 11 shows the ratio of the nominal computed critical depth, y_c, to the depth of tailwater, t_s, measured with respect to the level of the downstream edge of the shoulder at the upper limit of the transition range. The critical depth is defined by the equation

$$y_c = \sqrt[3]{\frac{q^2}{g}}, \tag{5}$$

wherein it is assumed that the flow is two-dimensional and the pressure is hydrostatically distributed in the vertical section.

Figure 12 shows, for free-flow conditions, the ratio of the critical depth to the depth of flow at the crown of the roadway, y_2. It appears that, in general, the depth at the crown is nearly equal to the nominal critical depth.

Free Discharge.--For free-discharge conditions the embankment acts as a control, and critical depth occurs on the roadway near the crown.

It follows that the theoretical discharge equation for flow over broad-crested weirs can be used as a basis for analyzing the one-dimensional discharge characteristics of the embankment. This equation is ordinarily written,

$$q = 3.09\ H^{3/2}, \tag{6}$$

where (H) is the total energy head measured to the control section, here taken to be the crown. The derivation of equation 6 is based on the assumption of potential flow (zero viscosity, no head loss), uniform velocity distribution, and hydrostatic pressure distribution. Thus, the total head is defined as

$$H = h + \frac{V^2}{2g} = h + \frac{q^2}{2g\ (P + h)^2} \tag{7}$$

As these conditions are never actually satisfied when real fluids flow over broad-crested weirs, a practical form of equation 6 is,

$$q = C\ H^{3/2}, \tag{8}$$

where (C), which depends on the form and roughness of the weir as well as the influence of viscosity, is determined by experiment. Equation 8 was used for the analysis of the free-discharge tests run in Series A to D. The unit discharge (q) in this equation was taken to be equal to the total discharge (Q) divided by the width of the flume (B). Figure 13 shows the results of these tests. Dashed portions of the curve drawn through Series A data were subsequently shown to be in error because of errors in discharge measurements. The trend shown by the check tests (Series C) is believed to be correct for this model. The difference between the curve

for Series B and that for Series A and C can be attributed to the influence of roughness. The decreasing positive slope of all the coefficient curves is believed to represent the decreasing influence of boundary resistance with increasing heads. The coefficient of discharge is plotted against the unit discharge in this figure because, for a given model and a given fluid, (q) is proportional to the Reynolds number (R).

Submerged Discharge.--For submerged flow over broad-crested weirs a satisfactory theoretical analysis has not been developed. In this report the influence of submergence is related to the submergence ratio, t/h, as defined in figure 2. The effect of submergence is represented by the ratio of the coefficient of discharge to the corresponding coefficient of free discharge for the same value of (q). In this instance, the coefficient is defined by the simple equations,

$$q = C_f h_f^{3/2} = C_s h_s^{3/2}, \tag{9}$$

where the subscripts (f) and (s) refer to the corresponding free and submerged-flow conditions for a given value of (q). Thus, the ratio of (C_s) to (C_f) is proportional to the ratio of the corresponding piezometric heads, or

$$\frac{C_s}{C_f} = \left[\frac{h_f}{h_s}\right]^{3/2}. \tag{10}$$

Figures 14, 15, and 16 show the results of submergence tests made in Series A, B, and D.

Accuracy of Data.--All measurements made for tests performed during the 1947-1949 period can be assumed to be reasonably accurate except the

discharge measurements for Series A. Inaccuracies revealed by subsequent investigations were remedied before tests in Series B and C were made. The model used for the Series A tests caused considerable difficulty because of surface distortion and dimensional changes. It is believed that this difficulty was largely overcome by the frequent determination of gage zeroes to prevent errors in elevation measurements. Nevertheless, the greater scatter in the data for this series reflects the inherent inadequacy of the first model set-up.

Because of its small size and certain construction details which were included as a result of the earlier experience, the model for Series D was generally superior to the 1:6-scale models. Superior instrumentation, too, partly accounts for the better accuracy which is believed to characterize the Series D tests.

Velocity traverses were taken in the three-foot flume with the model removed after completion of test Series C. The measurements indicated a distorted velocity distribution in the flume, with high velocities in the upper half and low velocities in the lower half of a section taken on the longitudinal centerline. In order to achieve similarity, the velocity distribution for the Series D tests in the 15-inch flume was made similar to that in the three-foot flume. The peculiar characteristics of the velocity distribution for all tests made in the 1947-1949 period can be expected to influence the results. The magnitude of this influence is indicated indirectly by comparisons of the writer's results with the results of the previous tests.

CHAPTER III

THEORETICAL CONSIDERATIONS

Free Discharge.--In the foregoing section the highway embankment is described as a form of broad-crested weir. For free-flow conditions it is assumed that critical depth will occur on the roadway at the crown. Ignoring the influence of boundary resistance and curvilinear flow, furthermore, equation 6 is a convenient one-dimensional equation of discharge. When real fluids flow over real embankments, however, the effects of boundary geometry and surface resistance require that this theoretical equation of discharge be modified. Equation 8, therefore, was defined as a practical discharge equation in which (C) for a particular form of embankment is a function of the geometric and fluid property variables represented by P/h, e/h, h/L_r, and $\underline{R}$ in equation 4. It is usually necessary that (C) be determined by experiment.

An alternative independent and practical expression for the discharge over an embankment is

$$q = 3.09\ k\ H^{3/2}, \tag{11}$$

where (k) is the ratio of the true discharge to the theoretical discharge given by equation 6. From equations 8 and 11,

$$k = \frac{C}{3.09}\ . \tag{12}$$

It follows that (k), like (C), is a function of boundary form, boundary roughness, and fluid viscosity.

The coefficient (k) is dependent on boundary form for two principal reasons. Equation 6, to which (k) is related by equation 11, is derived on the assumptions that the flow at the crown of the roadway is critical (specific energy is a minimum) and parallel (pressures are hydrostatically distributed in the vertical cross-section). Within the range of conditions tested on the basic embankment form used for this investigation, both of these assumptions appear to be substantiated to a remarkable degree (see figure 12, for example). However, because only one shape has been investigated it is assumed that, in general, the influence of boundary form must be evaluated experimentally.

The combined effects of boundary roughness and fluid viscosity are related to boundary resistance and energy losses due to internal shear. One of the important characteristics of real fluid flow which is associated with these influences is the existence of a growing boundary layer across the surface of the embankment and, therefore, a velocity gradient in vertical sections. Of particular interest in this connection is the concept of the discharge-displacement, boundary-layer thickness (δ^*).

In figure 17 (δ) is the nominal total thickness of the boundary layer, (U) is the uniform velocity in the potential region outside the boundary layer, and (u) is the mean velocity in the boundary layer at the distance (y) from the boundary. If (q_b) is described as the discharge in the boundary layer,

$$q_b = \int_o^{\delta} u \, dy \, , \tag{13}$$

or, in terms of the potential velocity and the discharge-displacement thickness,

$$q_b = U \, (\delta - \delta^*) \, . \tag{14}$$

Equation 14 is a definitive expression for (δ^*), which can be described as the distance which the boundary would have to be displaced to satisfy the equation of continuity if the velocity in the boundary layer were taken equal to (U). From equations 13 and 14,

$$\delta^* = \int_o^{\delta} (1 - \frac{u}{U}) \, dy \, , \tag{15}$$

which can be evaluated only if an analytical relation exists between (u) and (y). The total discharge in any vertical section of total depth (y_s) at a distance (s) from the nominal beginning of the boundary layer is, therefore,

$$q = U \, (y_s - \delta_s^*) \, . \tag{16}$$

The product ($U \, y_s$) in equation 16 is the discharge which would occur at this section if there were no boundary layer; that is, if the flow were potential. In other words, ($U \, y_s$) is equivalent to the theoretical discharge over the embankment given by equation 6.

The coefficient (k) has been defined as the ratio of the true discharge to the theoretical discharge. It follows that, in terms of the total depth at the crown, which in figure 17 is designated section 2,

$$k = \frac{U \, (y_2 - \delta_2^*)}{U \, y_2} = 1 - \frac{\delta_2^*}{y_2} \, . \tag{17}$$

Furthermore, if (y_2) is assumed to be equal to 2/3 H, which is in agreement with the assumption that critical depth occurs at or close to the crown, it follows that

$$k = 1 - \frac{3}{2} \frac{\delta_2^*}{H} \, . \tag{18}$$

Thus, equation 11 can be written

$$q = 3.09 \left(1 - \frac{3}{2} \frac{\delta_2^*}{H} \right) H^{3/2} . \qquad (19)$$

From dimensional analysis it is anticipated that, for a given form of embankment,

$$\frac{\delta_2^*}{H} = f_5 \left(\frac{e}{h} , \frac{h}{L_r} , \underline{R} \right) . \qquad (20)$$

Equation 19 is preferable to equations 8 or 11 as a practical discharge equation only if the assumptions made in its derivation are reasonably correct and only if (δ_2^*) can be computed from theoretical considerations. It follows that it is pertinent to review certain theories regarding the growth of the turbulent boundary layer in accelerated flow.

The Boundary Layer in Accelerated Motion.--The most practicable solution for the boundary layer on an embankment surface is derived from the so-called von Kármán momentum equation. An excellent review of the assumptions and operations involved in this derivation is given by Schlichting (6). Von Kármán's equation is based on the application of the momentum flux principle to the flow in the growing boundary layer. It presumes a hydrostatic normal pressure distribution and ignores the change in momentum due to the turbulence components of the total velocity. As applied to the turbulent boundary layer, it constitutes a semi-empirical solution which has been reasonably well substantiated for flat plates and circular pipes.

The von Kármán equation is usually written

$$\frac{\tau_o}{\rho U^2} = \frac{d\theta}{ds} + (2 + \frac{\delta^*}{\theta}) \frac{\theta}{2U^2} \frac{dU^2}{ds}, \tag{21}$$

where (τ_o) is the shear stress at the boundary, (s) is distance in the direction of the mean motion, and (θ) is the momentum-displacement, boundary-layer thickness,

$$\theta = \int_0^{\delta} \frac{u}{U} \left(1 - \frac{u}{U} \right) dy. \tag{22}$$

For intermediate values of the Reynolds number in open channels such as are involved in this investigation, experiments (7) (8) have indicated that the velocity distribution is best described with an equation of the power form,

$$\frac{u}{U} = (\frac{y}{\delta})^n \tag{23}$$

If equation 23 is substituted in equations 15 and 22,

$$\delta^* = \frac{n \delta}{n + 1}, \tag{24}$$

$$\theta = \frac{n\delta}{(n + 1)(2 n + 1)} = \frac{\delta^*}{2 n + 1}, \tag{25}$$

and it follows that the von Kármán equation can be written

$$\frac{\tau_o}{\rho U^2} = \frac{1}{2 n + 1} \frac{d \delta^*}{ds} + (\frac{2 n + 3}{2 n + 1}) \frac{\delta^*}{2U^2} \frac{dU^2}{ds}. \tag{26}$$

The left-hand member of equation 26 is a dimensionless shear coefficient which is ordinarily evaluated by semi-empirical methods based

on the assumption of a zero pressure gradient in the direction of motion. Granville (9) has shown that the sufficiency of these methods to approximate the shear in a flow with a convective pressure gradient depends only on the velocity distribution in the boundary layer. Rivas and Shapiro (10), furthermore, state that " ... in the region of (relatively) thin boundary layers the pressure gradient has a virtually negligible effect on the velocity profile and the rate of growth of the boundary layer." It appears that, in the present instance, the influence of the pressure gradient on (τ_o) can be ignored.

Within the intermediate range of values of the Reynolds number the boundary shear stress in smooth pipes and smooth flat plates with a zero pressure gradient is given by the empirical formula attributed to Blasius,

$$\tau_o = 0.0225 \left(\frac{U\delta}{\nu}\right)^{-0.25} \rho U^2 . \qquad (27)$$

The numerical coefficients in equation 27 are based on a velocity distribution which is given by equation 23 with (n) equal to 1/7. Bauer (7) and Delleur (8) have substantiated the use of the Blasius equation and the 1/7-power velocity distribution for flows in steeply sloping open channels and over broad-crested weirs.

If the 1/7-power assumption is extended to equation 24,

$$\delta^* = \frac{\delta}{8} \qquad (28)$$

and, from equation 27,

$$\frac{\tau_o}{\rho U^2} = 0.0134 \left(\frac{U\delta^*}{\nu}\right)^{-0.25} \qquad (29)$$

If equation 29 is substituted in the left-hand member of equation 26 and the 1/7-power assumption is also used to evaluate the right-hand member, the von Kármán equation becomes,

$$\left(\frac{\nu}{U\,\delta^*}\right)^{0.25} - 58.1\,\frac{d\delta^*}{ds} - 95.4\,\frac{\delta^*}{U^2}\,\frac{dU^2}{ds} = 0\,. \qquad (30)$$

Within the limits of the assumptions made in its derivation equation 30 should be applicable to the boundary layer on the surface of smooth embankments. However, it is not yet possible to integrate this equation to obtain (δ_2^*) in the discharge equation. In the first place, the virtual origin of the boundary layer indicated on figure 17 is indeterminate. The nominal origin, for convenience of reference and measurement, is taken to be the upstream edge of the shoulder. Actually, of course, a layer of finite thickness exists at the latter point. Similarly, several uncertainties are involved in the existence of a separation zone just downstream from the intersection of the upstream embankment and shoulder slopes. It is reasonable to assume that one effect of the separation zone is to initiate turbulence which would virtually eliminate the possibility of a laminar boundary layer downstream from that point. It can be anticipated, also, that the boundary layer will be displaced an amount approximately equal to the thickness of the separation zone. This would result in an apparent boundary-layer thickness in this zone which would be greater than the actual thickness. Furthermore, the velocity pattern and, therefore, the shear stress and rate of growth of the boundary layer are certainly influenced by the occurrence of the separation zone. On the other hand, the flow in the region near the separation zone, and at the free surface

in the same section, is curvilinear--a condition which contradicts one of the basic assumptions in the foregoing derivations.

A second major obstacle to the integration of equation 30 is related to the fact that the third member of the equation represents the influence of the convective acceleration over the embankment surface. It is apparent that the velocity gradient term in this member will depend on experimental evaluation. It is not apparent, however, whether the result will be an integrable function.

It should also be observed that the derivation of equation 30 ignores the influence of surface roughness. It follows, therefore, that the equation is applicable only to smooth surfaces. Lack of time and the resulting paucity of data on the effect of roughness in the writer's experimental investigation make it impractical to extend the theoretical discussion to this problem.

As an indication of the integral equations which might define the limits of equation 30, two cases are considered: (1) The flow is assumed to be non-accelerated; that is, $dU^2/ds = 0$, and (2) the velocity head in the zone outside the boundary layer is assumed to be directly proportional to the distance from the origin of the boundary layer; that is, $dU^2/ds = U^2/s$. In both cases it is assumed that $\delta = 0$ when $s = 0$.

Thus, if $dU^2/ds = 0$, simple integration gives

$$\frac{\delta^*}{s} = 0.0462 \left(\frac{Us}{\nu}\right)^{-0.20} \tag{31}$$

On the other hand, if $dU^2/ds = U^2/s$, an approximate integration gives

$$\frac{\delta^*}{s} = 0.019 \left(\frac{Us}{\nu}\right)^{-0.20} . \tag{32}$$

Submerged Discharge.--The scope of the writer's investigation does not include a detailed study of the internal characteristics of submerged flow. Much of what is said in the foregoing discussion pertains to both free and submerged flow, however.

The method of analysis presented in Chapter II for the 1947-1949 tests is also used for the analysis of the writer's data. In equation 10 the ratio C_s/C_f is defined as a ratio which indicates the relative influence of tailwater submergence. From equation 4, it is anticipated that this ratio is functionally represented by the equation,

$$\frac{C_s}{C_f} = f_6 \left(\frac{P}{h}, \frac{e}{h}, \frac{h}{L_r}, \frac{t}{h}, \underline{R} \right) . \qquad (33)$$

None of the ratios contained in equation 33 can be eliminated as independent variables unless the experimental results indicate that their influence is negligible. In the presentation of the submerged-flow test results, (t/h) has been selected as the principal independent ratio.

CHAPTER IV

LABORATORY SET-UP

General Arrangement.--The laboratory tests for the writer's investigation were made in the Hydraulics Laboratory, School of Civil Engineering, Georgia Institute of Technology. The general arrangement of the experimental equipment is shown in figures 18 and 19. The embankment model was located in an existing flume. Water was supplied to the flume from the laboratory's constant-head recirculating system. A gate valve in the 12-inch supply line was used to regulate the discharge. The maximum capacity of the water system at this location is about 6.0 cubic feet per second.

The Flume.--The flume used for this investigation is three feet wide, three feet deep, and thirty feet long from baffles to tailgate. Baffles required to produce a uniform flow in the flume consisted of link-wire fencing at the inlet, a low weir, two wooden and corrugated metal cribs, two expanded-metal screens, and a surface float. A hinged tailgate provided for control of tailwater levels. Velocity profiles, measured at the upstream toe of the embankment, are shown in figure 20.

Adjustable rails on the top of the flume provided a level support for sliding point-gage and pitot-tube carriages.

The 1:9-Scale Model.--In order to be able to check and extend the results of the earlier tests the shape of the embankment section for the 1:9-scale model was made the same as the 1:6- and 1:12-scale models. The prototype dimensions of the basic design are shown on figure 1.

The principal elements of the framework for the 1:9-scale model were built of waterproof plywood. The embankment surfaces were also made of plywood, but the shoulder surfaces and both halves of the roadway surface consisted of separate, flat pieces of 1/4-inch polished aluminum plate. The construction tolerance for elevations was 0.001 foot and the tolerance for surface lengths was 0.005 feet.

False floors in the flume both upstream and downstream from the model provided for varying the relative height of the embankment. Only two different heights were investigated in the writer's tests, however.

Surface roughness was achieved by stretching a length of new 14 x 18-mesh standard bronze window screen over the complete embankment section. The diameter of the wire from which the screen was made was 0.011 inches. The sand-grain equivalent of this kind of roughness was not determined. Bauer (7), using a 16 x 16-mesh screen made of 0.010-inch diameter wire, estimated that it had a roughness value comparable to that of rough concrete. Subsequent analysis by Bauer and Halbronn (11) indicated that the effective roughness was somewhat less, however.

Discharge Measurements.--The rate of flow for all of the writer's tests was determined from weighing measurements. The laboratory's main weighing tank is located below the flume in which the model was located. It has a maximum water capacity of 15,000 pounds, and it is equipped with automatic controls to move the diversion car, open and close the tank valve, and start and stop an electric time-interval clock. The overall accuracy of the equipment is believed to be such that the discharge measurements are accurate to about one-half of one per cent.

Piezometric-Head Measurements.--The elevations of the headwater and tailwater with respect to the crown of the roadway were measured with hook-gages mounted over transparent stilling wells connected to wall or floor piezometers. The locations of the piezometers are shown on figure 18, and the hook gages mounted on the side of the flume are shown in figure 19. These gages were zeroed by means of an engineer's transit and a special, light-weight target rod. Both measurements are believed to be accurate to 0.001 foot.

Water-surface profiles were measured with a point gage mounted on a movable carriage. This gage is shown on the left in figure 21. The headwater level, as measured by the hook gage, was used to zero the point gage. Longitudinal stationing for the measurements was determined from a steel tape located adjacent to the slide rail on the top of one of the flume walls. The accuracy of the profile measurements depended on the irregularity of the water surface at the station of measurement. In general, however, it is believed that the surface elevations were measured to 0.002 feet.

Velocity Measurements.--Velocities outside the boundary layer were measured with a pitot-static tube mounted on a sliding carriage. This tube, which is shown on the right in figure 21, is a standard instrument in the Georgia Tech Hydraulics Laboratory. Its outside diameter is 3/16-inch and the stagnation and static openings are located so that the coefficient of the tube is very nearly 1.0. The air-water differential manometer used for the pitot-static tube is shown on figure 22. This manometer is of the zero-displacement type, with back-lighted stainless-steel needles in glass tubes for positioning the menisci. The smallest division on the vernier for this gage was 0.001 foot.

The stagnation tube used for boundary-layer velocity measurements is shown in figure 23. The stagnation tip on this tube is a 22-gauge (0.028 inches diameter) stainless-steel hypodermic needle. The vertical leg is a brass tube 1/8 inch in diameter, backed up with a streamlined brass bar. The tube is mounted on a hook-gage frame. Accurate positioning of the tube was determined with a dial-type displacement gage attached to the hook-gage staff. The smallest division on the dial was 0.001 inches. The depth-measurement gage zero for the stagnation tube was determined at each measuring station by setting the dial gage to read zero when the bottom of the tube was placed against the surface of the model without bearing any of the weight of the tube assembly. The tip of the tube was accurately located in this position by means of a horizontal light beam focussed through the glass wall of the flume from a position opposite the observer and at an elevation just above the surface. The tube was positioned very sensitively by lowering it until no light could be seen between the needle and the polished surface of the model. The stagnation-tube staff was provided with a pivot mount in order that depth traverses could be taken in a section which was perpendicular to the surface of the model at all stations.

The manometer used for the stagnation-tube measurements, shown in figure 24, is essentially a zero-displacement point gage. It consists of a back-lighted needle in a small glass tube mounted on a frame which utilizes a precise vernier caliper for elevation determinations. The smallest division on the vernier corresponded to a difference in elevation of 0.001 inch. The zero reading for velocity measurements with the stagnation tube was determined by comparison with the differential reading

obtained with the pitot-static tube in a uniform flow zone outside the boundary layer. It follows that the accuracy of velocity measurements in the boundary layer depends on the accuracy of the pitot-static tube measurements.

CHAPTER V

EXPERIMENTAL PROCEDURE AND TEST RESULTS

Scope of the 1:9-Scale Tests.--The writer's experimental program consisted of three series of tests, designated Series E, F and G, all of which were performed on the 1:9-scale model of the embankment section shown in figure 1. These tests were intended primarily to extend the results of the previous tests. Data were obtained which provide additional information on free- and submerged-flow discharge coefficients, the influence of surface roughness, and the transitions between various flow regimes. It was the purpose of one series of tests to provide limited information on the influence of embankment height. In addition, velocity measurements were made which furnish a limited amount of original data on the acceleration of the mean flow and the growth of the boundary layer over the roadway. Some of the factors which influence the transition between plunging and surface flow were revealed in a few special tests.

A summary of the principal model characteristics involved in Series E, F and G is given in table 2.

Table 2. Summary of the 1:9-Scale Tests

Series	Surface	Height (P)
E	smooth (aluminum)	10.5 ft (prototype)
F	rough (screen)	10.5
G	smooth (aluminum)	5.25

The discharge equations in Chapters II and III were derived for two-dimensional flow. In other words, (q) is defined as the discharge over a

typical one-foot length of roadway. The laboratory tests, on the other hand, were made in a three-foot wide flume. It is acknowledged that the existence of a boundary layer at both wall boundaries and the possible existence of secondary flow over the roadway may result in an erroneous indication of the two-dimensional discharge characteristics. Delleur (8), for example, has found such effects to be appreciable in broad-crested weir experiments. For most of the writer's tests, however, the aspect ratio (ratio of head to width of flume) was very small, and it is believed that the relative effect of these influences is small. Nevertheless, this is a topic which deserves attention in future investigations.

Free-Discharge Tests.--Tests to determine the free-flow discharge coefficient involved the measurement of the headwater level and the discharge. The temperature of the water was also recorded for each test. The discharge coefficient was computed from equation 8, wherein (q) was taken to be equivalent to the total discharge (Q) divided by the width of the flume (B).

Figure 25 shows the results of the free-discharge tests for Series E, F and G. In this figure (C) is plotted as a function of the unit discharge because (q) is proportional to the Reynolds number (R). Thus, the shape of the curves indicates the relative influence of viscosity on the discharge function.

Submerged-Discharge Tests.--Tests to determine the effect of tailwater submergence involved the measurement of the tailwater level in addition to the headwater level and the discharge. The results of the writer's tests, analyzed on the basis of equation 10, are shown in figures 26, 27

and 28 for Series E, F and G, respectively. In each of these figures (C_s/C_f) is shown as a function of the submergence ratio, (t/h). A single average curve is drawn through the test points on each figure.

Description of the External Flow Pattern.--The writer's experimental program did not include as many measurements of the external flow pattern characteristics as were involved in the previous tests. No complete surface profiles were taken, but the observations required to define the various flow regimes indicated on figure 7 were made for a full range of test conditions in each series.

The transition from free to submerged flow is designated the point of incipient submergence. In these tests, as in the previous tests, this transition point was determined by holding the discharge constant, gradually raising the tailwater, and observing the tailwater level at which the headwater level first begins to rise due to submergence. The point of incipient submergence is well defined, and is the same for falling tailwater as it is for rising tailwater levels. On figures 26, 27 and 28 it is indicated as the intersection of the submergence curves with the line $C_s/C_f = 1.0$.

The free-flow transition range, marking the limits of the plunging- and surface-flow regimes, was determined visually. In a typical test, with discharge constant, the tailwater was gradually raised until plunging flow changed abruptly to surface flow. The tailwater level at which this transition took place was recorded as the upper limit of the range. The tailwater was then lowered slowly until surface flow changed to plunging flow. This is the lower limit of the range. Some of the distinctive characteristics of the changing flow pattern are shown in figures 8 and 9.

The limits of the transition range for Series E, F and G tests are shown on figures 29 and 30. The ratio of the critical depth (y_c) to the depth (t_s) at the upper limit of the transition range is shown on figure 31. The depth (t_s) is the depth of the tailwater referred to the level of the downstream edge of the shoulder. A definition sketch is shown on figure 11.

Velocity Measurements.--Detailed velocity measurements were made for three different free discharges in Series E. Additional measurements were made for one discharge in Series E and one in Series F. A summary of the principal test conditions for these measurements is given in table 3.

Table 3. Summary of Velocity-Measurement Tests

Test	Series	Surface	q	y_2	Number of Traverses
1	E	smooth	0.863	.292	6
2	E	smooth	1.557	.424	6
3	F	rough	0.771	-	1
4	E	smooth	0.155	.091	4
5	E	smooth	0.293	-	1

All velocity measurements were made on a longitudinal section which was approximately on the centerline of the flume. The longitudinal stationing for these measurements appears on the surface of the model in figure 21. The zero for the stationing was taken to be the junction of the upstream embankment and the shoulder. The crown of the roadway, therefore, was at station 1.67. Depth stationing for velocity traverses was referred to the surface of the model. The procedure used to determine the zero readings for depth stationing is described in Chapter IV. Boundary-layer traverses were taken on a line which was perpendicular to the surface of

the model at each section. Outside the boundary layer the tube was visually aligned to be approximately parallel to the flow for each measurement. Stagnation tube readings were converted to velocities by comparison with pitot-static tube measurements at corresponding points outside the boundary layer.

Detailed velocity traverses involved a complete stagnation-tube survey through the boundary layer and several pitot-static tube measurements outside the boundary layer. For tests 1, 2 and 4, as shown on figures 32, 33 and 34, detailed traverses were made at several stations between the upstream edge of the shoulder and the crown of the roadway. For Test 2, two traverses were made at stations downstream from the crown. For Tests 3 and 5 complete traverses were made only at a station near the crown of the roadway. The measurements for Tests 3 and 5 are shown in figure 35. A summary of the velocity measurements outside the boundary layer for Tests 1, 2 and 4 is shown on figure 36.

CHAPTER VI

ANALYSIS AND DISCUSSION OF RESULTS

Characteristics of the Boundary Layer.--The solution of equation 19 for free, two-dimensional flow over smooth embankments requires knowledge of the discharge-displacement, boundary-layer thickness at the crown of the roadway, δ_2^*. Integration of equation 26 to get (δ_2^*), on the other hand, requires (1) that the exponent (n) in the velocity equation be known, (2) that the virtual origin of the boundary layer be known, and (3) that the term which represents the influence of convective acceleration be known and integrable. The information required to satisfy these three requirements must be obtained from the results of experiments. These restrictions are added to the requirement that all the assumptions made in the derivation of the von Kármán equation must be satisfied.

Figures 32, 33, 34 and 35 show the results of velocity traverses in the boundary layer on the surface of the embankment. Only the first three figures include enough stations to describe the growth of the boundary layer. Figure 35(a) shows a single traverse near the crown with the screen roughness on the surface of the model. All other traverses were made with free flow over the smooth aluminum surface. Tests 1 and 2 shown on figures 32 and 33 appear to substantiate the use of the 1/7-power velocity distribution except in the immediate vicinity of the separation zone at the upstream edge of the shoulder and in the region downstream from the crown. Test 4, figure 34, was made with a very low discharge. This test indicates a trend toward the 1/7-power distribution which is

strangely contradicted at station 1.6. Test 5, figure 35(b), shows a single traverse at the same station and with a low discharge. The results of Test 5 indicate a probable error in the measurements made at station 1.6 for Test 4.

On the basis of the limited data shown in figures 32 to 35, inclusive, it is reasonable to assume that the velocity distribution over most of the roadway surface upstream from the control section can be represented approximately by the 1/7-power equation. It follows that the von Kármán equation for the growth of the boundary layer can be expressed by equation 30.

Two major prerequisites remain before equation 30 can be integrated to obtain (δ_2^*). The first of these is the knowledge of the virtual origin of the boundary layer. There appears to be no satisfactory way to establish this point without knowledge of the theoretical form of the boundary-layer growth curve. On the other hand, the form of the boundary layer depends on the second of the remaining prerequisites for integration, which is the knowledge of the convective acceleration in the flow outside the boundary layer. These conflicting requirements lead to the conclusion that integration must be accomplished by a successive approximations procedure.

Experimental data on the growth of the boundary layer are shown on figure 37(a). In this figure the boundary-layer thickness is plotted as a function of the distance from the nominal origin at the upstream edge of the shoulder as shown on figure 17. The data plotted were obtained from the velocity profiles shown on figures 32 to 35, inclusive. The nominal boundary-layer thickness, δ, is taken to be the depth at which the vertical,

potential-velocity curve on these figures intersects the sloping line which represents the velocity distribution in the boundary layer. This appears to be the best method of determining (δ), although its accuracy depends considerably on the graphical fitting of the average curves to the test points on the velocity diagrams. Within the range of accuracy of the data, the points representing Tests 1 and 2 appear to define a single curve. Points representing the low-discharge tests, 4 and 5, however, define a lower curve. Average curves drawn through the test points indicate a rapid growth of the boundary layer over the shoulder and a slower growth over the roadway. At station 1.6, which is only 0.07 feet upstream from the crown, Tests 1, 2 and 5 show a deviation from an average value of (δ) which is not greater than the expected experimental error. The measurement for Test 4 at this station is believed to be in error. Thus, an average value of (δ_2) for the full range of discharge involved in figure 37(a) is about 0.32 inches or 0.027 feet.

Equations for (δ) as a function of (s) are readily derived from equations 31 and 32 in combination with equation 28. Thus, for the condition that $dU^2/ds = 0$, which is the case of non-accelerated flow,

$$\delta = 0.37\ s\ \left(\frac{Us}{\nu}\right)^{-0.20} \qquad (34)$$

For the condition that $dU^2/ds = U^2/s$,

$$\delta = 0.152\ s\ \left(\frac{Us}{\nu}\right)^{-0.20} \qquad (35)$$

Curves representing equations 34 and 35 (using values of (U) measured for Test 1 as typical) are shown on figure 37(a) for comparison with the experimental data. It is believed that, if equation 30 is assumed to

be a reasonably good expression for the growth of the boundary layer on the embankment surface, the theoretical curve corresponding to the test points would lie somewhere between the curves representing equations 34 and 35. Thus, if the form of the theoretical curve were known, it could be displaced to the left, as indicated by curve B' on figure 37(b), until it fitted the experimental data. The virtual origin would then be indicated as the abscissa of the origin of the transposed theoretical curve. However, the curves representing equations 34 and 35 both show a tendency to become asymptotic to a straight line which has a greater positive slope than the curves which join the experimental data. It is unlikely, therefore, that a theoretical curve which is similar in form to the curves for equations 34 and 35 would fit the test points. To illustrate this conclusion, the difference between a transposed theoretical curve (B') and a test curve (A) is indicated in figure 37(b) as a shaded area. It is suggested that the disagreement with theory represented by the shaded area is largely the result of the boundary-layer displacement and the associated disturbance due to the occurrence of a separation zone at the upstream side of the shoulder. Such an effect was anticipated in Chapter III. Unfortunately, the data available from the writer's experiments are insufficient to define either the size of the separation zone or its influence on the flow pattern.

An integrable function describing the convective acceleration in the region outside the boundary layer has been described as the second of the remaining prerequisites for integrating equation 30. Figure 36 shows the results of velocity measurements made outside the boundary layer for Tests 1, 2 and 4. Straight lines fit the points for each of the three

tests, suggesting that the velocity in the potential zone varies directly with distance. The circled points on figure 36 show values of (U) computed on the basis of potential flow between the headwater and the embankment, or

$$U = \sqrt{2g\,(H - h_s)}\,, \tag{36}$$

where (h_s) is the piezometric head referred to the crown at any distance (s) from the origin. The good agreement between the computed and measured values of (U) over the roadway substantiates the assumption that the head loss in the region outside the boundary layer, between the headwater and the control section, is negligible. The lack of agreement between the two curves near the upstream end of the embankment probably reflects the influence of the curvilinear flow in this region on the pitot-static tube measurements.

The straight lines on figure 36 for Tests 2 and 4, representing the maximum and minimum discharges, respectively, are parallel. The slope of these lines is $dU/ds = 0.058$ units per second. An approximate empirical expression for (U) for the full range of the tests is, therefore,

$$U = U_o + \frac{dU}{ds}\, s = U_o + 0.058\, s, \tag{37}$$

where (U_o) is the velocity at $s = 0$. Substituted in equation 30, equation 37 would not yield a simply integrable expression. Although it is reasonable to believe that the integration could be accomplished by an approximation procedure, the lack of data regarding the location of the virtual origin of the boundary layer is added reason to forego any attempt to integrate equation 30 at this time.

The Discharge Equation.--The proposed two-dimensional free-discharge equation, equation 19, involves the theoretical coefficient 3.09 and a correction term which depends on the relative magnitude of the discharge-displacement, boundary-layer thickness at the crown. For this equation to be of general significance it is necessary that it be possible to compute (δ_2^*) for all values of discharge and roughness and all forms and sizes of embankments. In the preceding section it is concluded that sufficient data are not available to substantiate a suggested approximate procedure for solving the boundary-layer equation. This indicates the need for an extension of the writer's work, of course. It is nevertheless possible to test the validity of the discharge equation as it applies specifically to the writer's test conditions.

A check on the validity of equation 19 as an independent discharge equation involves the substantiation of the equation

$$\frac{C}{k} = 3.09 \tag{38}$$

from equation 8 and 11. From equation 8,

$$C = \frac{q}{H^{3/2}} . \tag{39}$$

Also,

$$k = 1 - \frac{3}{2} \frac{\delta_2^*}{H} . \tag{18}$$

In these equations δ_2^*, H, and (q) are independently measured experimental quantities. Actually, of course, the writer's experiments did not involve a direct measurement of the unit discharge. Because his tests

were performed in a three-foot-wide flume, not (q) but the total discharge (Q) was measured. However, if (δ^*_b) is defined as the discharge-displacement, boundary-layer thickness at the side walls,

$$q = \frac{Q}{B - 2\,\delta^*_b} \tag{40}$$

in which (B) is the measured width of the flume. The scope of the writer's work did not include an investigation of the magnitude and influence of (δ^*_b). It might be assumed, however, that (δ^*_b) is commensurate with (δ^*_2). In a preceding paragraph a value of 0.027 feet was suggested as an average value of (δ_2) for all of the boundary-layer measurements on the smooth-surface model. From equation 28, the corresponding value of (δ^*_2) is approximately 0.003 feet. The error in the computation of (q), therefore, is indicated by the ratio,

$$\frac{Q/B}{Q/(B - 2\,\delta^*_2)} = \frac{3 - 2(0.003)}{3} = 0.998.$$

In other words, the error in (q) which results from neglecting (δ^*_2) is approximately 0.2 per cent. This is considerably less than the experimental error to be expected. It follows that the values of (C) shown on figure 25, which were computed without regard for the effect of the side-wall displacement thickness, are used in the evaluation of equation 38.

In the foregoing paragraph the value $\delta^*_2 = 0.003$ feet was selected as an approximate, average value for Tests 1, 2, 4 and 5. If this value is substituted in equation 18,

$$k = \left(1 - \frac{0.005}{H}\right), \tag{41}$$

which was used for all Series E tests on the smooth-surfaced embankment.

Only one boundary-layer traverse (Test 3) was made on the rough-surfaced model, Series F. For this test, from figure 35(a), (δ_2) is 0.54 inches and (n) is estimated to be 1/3.1. From equation 24, therefore, the corresponding value of (δ_2^*) is 0.132 inches, or

$$k = \left(1 - \frac{0.017}{H} \right) . \qquad (42)$$

As an approximation of the effect of (δ_2^*) on all tests with the rough boundary, equation 42 was used for the tests in Series F.

No velocity traverses were made to establish the boundary-layer characteristics for the Series G model. It seems reasonable, however, to use equation 41 as an approximation for (k) for the tests made in this series. The only difference in the models for Series E and G was in the embankment height (P), as shown in table 2.

Values of the ratio C/k for all of the writer's free-discharge tests are shown on figure 38 as a function of (q). The remarkably well-defined curve for C/k = 3.09 at all but the lowest values of (q) is a gratifying substantiation of equation 19 within the limits of the experiments made by the writer. It is suggested that the deviation at the lower discharges is due to the fact that the actual value of (δ_2^*) for these tests might be considerably less than the average values used in equations 41 and 42. Experimental data shown in figure 37(a) for Test 4 indicate a trend toward decreasing values of (δ) for decreasing values of (q). Additional data will be required to substantiate this trend.

If the form of the boundary-layer equation represented by equations 34 and 35 is assumed to be applicable to the highway embankment, and if

such an equation could be derived by integration of equation 30 for the conditions of the writer's tests, it might be written,

$$\delta = A\, s\, \left(\frac{Us}{\nu}\right)^{-0.2} \qquad (43)$$

in which (A) is a constant. Equation 43 indicates that the boundary-layer thickness should increase as the Reynolds number, or the discharge, decreases. The opposite trend is indicated by the test results on figure 37(a). It is suggested that this contradiction is another influence of the separation zone which occurs near the upstream edge of the shoulder. As the discharge decreases, the size of the separation zone can be expected to decrease. As a result, the initial boundary-layer displacement at the separation zone also decreases. It seems reasonable that this occurrence might explain the experimental evidence of lower values of (δ) for lower values of (q).

In view of the uncertainties regarding the influence of scale and roughness on (δ_2^*), no attempt was made to check the validity of equation 19 applied to the 1:6- and 1:12-scale tests data shown on figure 13.

Submerged Discharge.--The influence of submergence, in terms of the coefficient of discharge for free discharge, is shown on figures 14, 15 and 16 for Series A, B, and D tests. Similar data for Series E, F and G are shown on figures 26, 27 and 28.

The ratio C_s/C_f is described in equation 33 as a function of P/h, e/h, h/L_r, t/h, and ($\underline{R}$) or (q). A definite correlation with (q) is shown on figure 15. This conclusion is generally substantiated in figure 14, but the data for Series D, E, F and G show such a small spread that no

such correlation is apparent. It appears from all of the available submergence tests that the influence of the h/L_r ratio is insignificant. Similarly, data from the 1:6- and 1:12-scale tests appear to eliminate P/h and e/h as independent variables. However, comparison of the average curves on figure 26, 27 and 28 indicates a significant influence due to both of these ratios. More experiments are needed to resolve the apparent contradiction regarding the relationship between C_s/C_f , P/h and e/h.

It is pertinent to observe that incipient submergence occurs at or near the point t/h = 0.85 for all of the tests made in Series A to G, inclusive.

Classification of the Free-Flow Transition Range.--Figures 10 and 11 show summaries of data which define the transition range for surface or plunging flow from the 1:6- and 1:12-scale model tests. Similar data for the 1:9-scale tests are shown in figures 29, 30 and 31. Figures 10, 29 and 30 show the tailwater limits for the transition range as a function of (q). The curves for each test series are well-defined, but there is little correlation between the different models.

Figures 11 and 31 show the tailwater level in terms of the critical depth at the upper limit of the transition range. In these figures, as in those described in the preceding paragraph, the data for each series of tests define a curve, but the curves for the different models show no reasonable correlation with the known variables. A probable explanation for the apparent inconsistencies is suggested from the results of a few special tests, shown on figure 31(a), which were made after the completion of most of the writer's work.

All the unnumbered points shown on figure 31(a) for the Series E model are taken from the results of tests made in one period shortly after the construction of the 1:9-scale model was completed. Subsequently, in preparing the model for the boundary-layer measurements, the surface of the model was smoothed and polished. At this time it was discovered that swelling of the plywood used for the embankments had caused an edge of the downstream embankment surface to project above the downstream edge of the shoulder plate. The projection was removed, therefore, before an additional, needed transition-range test was made. The result of this test is shown as point 1 on figure 31(a). Because this point was so far removed from the average curve, a check test was made. This point is shown as point 2, which appears to substantiate the experimental accuracy of point 1. It was then suggested that the removal of the small shoulder projection might have accounted for the discrepancy between points 1 and 2 and all the other data shown on this figure. Thus, a third test was made with a straight wire of 0.09-inches diameter fastened to the downstream edge of the shoulder. The result of the test is indicated on figure 31(a) as point 3.

The three special tests are also shown on figure 29, and the marked influence due to the shoulder projection is apparent. It is concluded, therefore, that the limits of the transition range are appreciably affected by the form of the downstream shoulder. Of course, because the control section is at or near the crown, the free-discharge coefficient is unaffected by such slight variations in the geometry of the downstream side of the embankment.

Figure 12, based on the Series A, B, C and D tests, shows data which define the relationship between the depth at the crown and the

computed critical depth (equation 5). For all of the tests, and especially for the Series D tests--which are believed to be the most accurate--the ratio is remarkably close to 1.0 over the range of conditions tested. This agreement with one of the basic assumptions is doubtless one of the reasons for the apparent validity of the discharge equation.

CHAPTER VII

CONCLUSIONS

1. Experiments on a single form of embankment have substantiated the free-discharge equation

$$q = 3.09 \left(1 - \frac{3}{2} \frac{\delta_2^*}{H} \right) H^{3/2} \qquad (19)$$

where (δ_2^*) is the discharge-displacement boundary-layer thickness at the crown and (H) is the total head measured with respect to the level of the crown.

2. Additional experimental data are required in order to be able to compute (δ_2^*) for all forms and sizes of embankments. To the extent that these data become available, equation 19 will become a general, semi-analytical equation of discharge.

3. Data are especially needed (a) to define the magnitude and nature of the influence of the separation zone which forms at the intersection of the upstream embankment and shoulder surfaces, (b) to establish the virtual origin of the boundary-layer, (c) to determine an integrable expression for the convective-acceleration term of the boundary-layer growth equation, and (d) to describe the influence of boundary roughness.

4. The velocity distribution in the boundary layer over the roadway can be described by a 1/7-power equation.

5. The influence of submergence is primarily a function of the tailwater-head ratio. Minor influences are related to the embankment-

height-head ratio and the relative-roughness ratio. The point of incipient submergence occurs, in general, when the tailwater head (t) is about 0.85 times the upstream piezometric head (h).

6. The upper and lower tailwater limits which define the transition from plunging flow to surface flow are well defined for a given model. The transition range is very sensitive to small details of form on the downstream shoulder.

REFERENCES

1. Yarnell, David L., and Nagler, Floyd A., "Flow of Water over Railway and Highway Embankments," Public Roads, Vol. 11, No. 2, April 1930, pp. 30-34.

2. Horton, Robert E., "Weir Experiments, Coefficients, and Formulas," Water-Supply Paper No. 200, U.S. Geological Survey, 1907.

3. Woodburn, James G., "Tests of Broad-Crested Weirs," Transactions, American Society of Civil Engineers, Vol. 96, 1932, pp. 387-453.

4. Prentice, T. H., "Hydraulics of the Broad-Crested Weir," Master's thesis, Cornell University, 1935.

5. Ippen, Arthur T., "Channel Transitions and Controls," Chapter VIII, Engineering Hydraulics, edited by Hunter Rouse, John Wiley and Sons, 1950, p. 527.

6. Schlichting, H., "Boundary Layer Theory," Technical Memorandum No. 1217 (Part I) and No. 1218 (Part II). (Translation from the German), National Advisory Committee for Aeronautics, April 1949.

7. Bauer, William J., "Turbulent Boundary Layer on Steep Slopes," Transactions, American Society of Civil Engineers, Vol. 119, 1954, pp. 1212-1242.

8. Delleur, J. W., "Boundary Layer Development in Open Channels," Doctoral dissertation, Columbia University, 1955.

9. Granville, Paul S., "A Method for the Calculation of the Turbulent Boundary Layer in a Pressure Gradient," Report No. 752, David W. Taylor Model Basin, Navy Department, May 1951.

10. Rivas, Miguel A., Jr., and Shapiro, Ascher H., "On the Theory of Coefficients for Rounded Entrance Flow Meters and Venturis," Paper No. 54-A-98, Transactions, American Society of Mechanical Engineers Advance Copy, 1954.

11. Halbronn, G., "Turbulent Boundary Layer on Steep Slopes," a discussion of reference 7, pp. 1234-1240.

APPENDIX

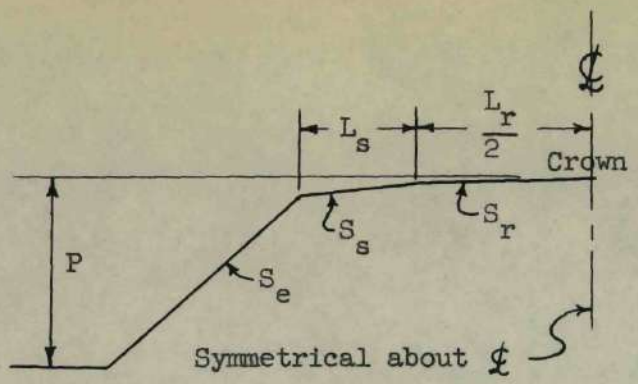

Basic Embankment Section.

P = 10.5 ft (except Series G)

P = 5.25 ft (Series G)

L_s = 6 ft - 0 in.

L_r = 18 ft - 0 in.

S_e = 1 on 2

S_s = 4-1/2 in. on 6 ft

S_r = 1-1/2 in. on 9 ft

(all dimensions shown as in prototype)

Fig. 1. DEFINITION OF BOUNDARY VARIABLES.

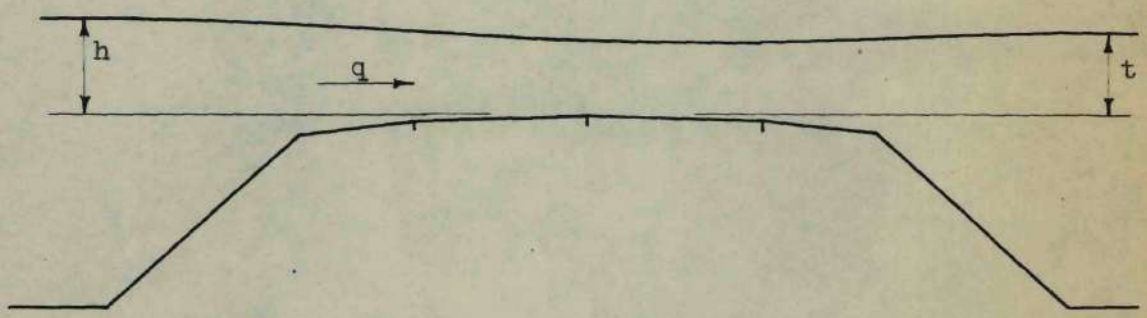

Fig. 2. DEFINITION OF FLOW VARIABLES.

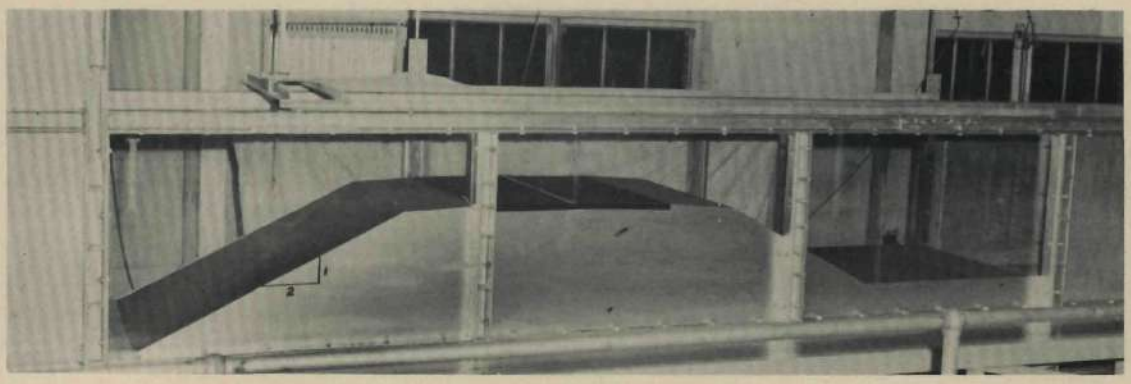

Figure 3. General View of 1:6-Scale Model.

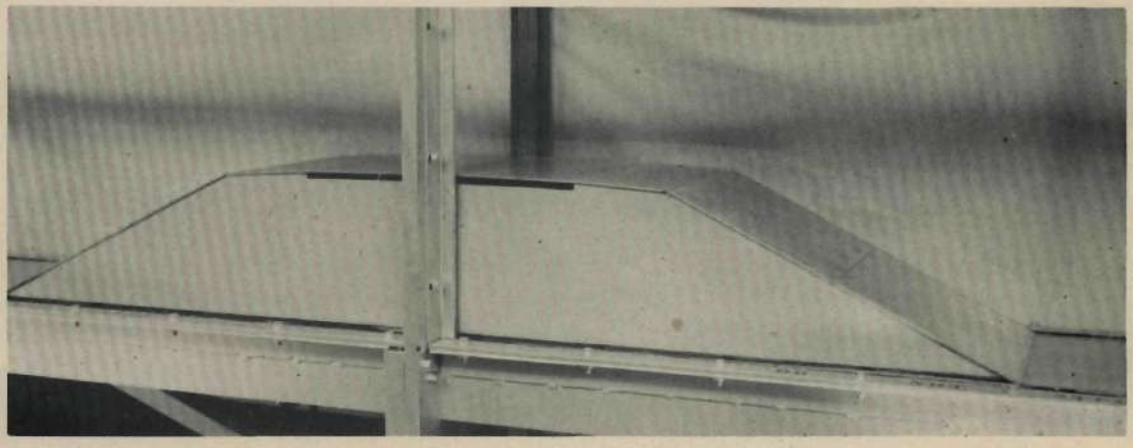

Figure 4. General View of 1:12-Scale Model.

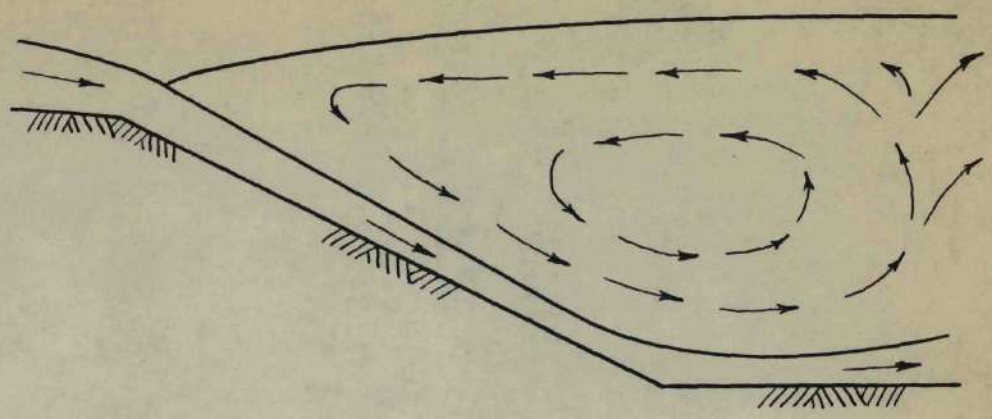

(a) Plunging (Free) Flow.

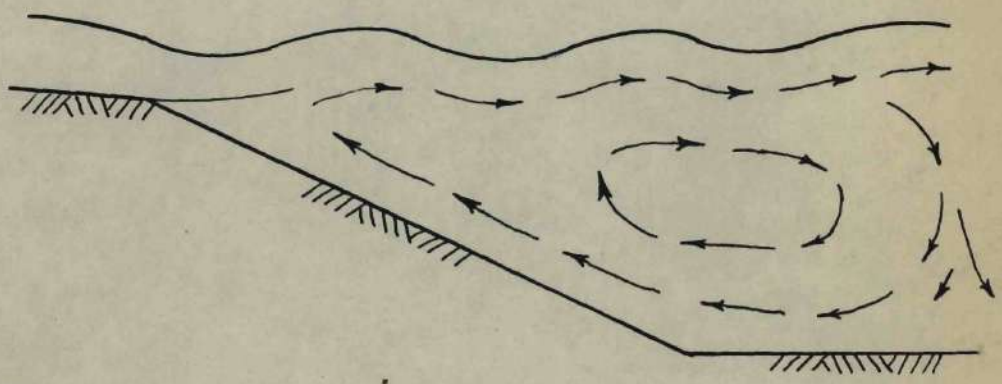

(b) Surface (Free) Flow.

Fig. 5. SUB-CLASSIFICATION OF FREE FLOW.

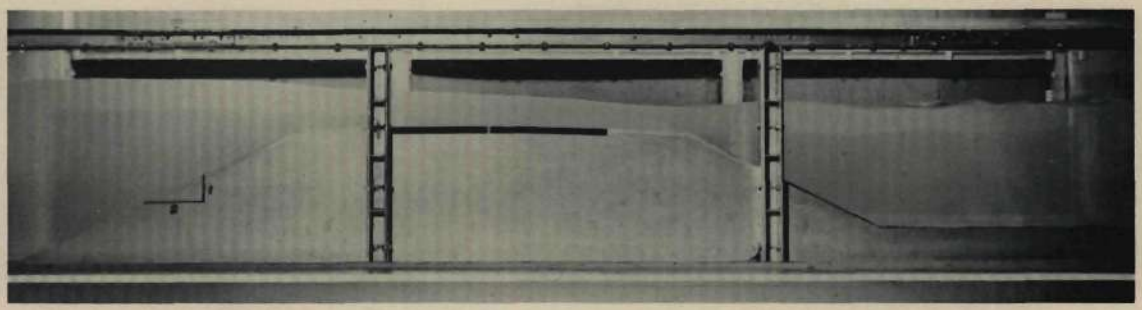

(a) FREE (SURFACE) FLOW AT THE UPPER LIMIT OF THE TRANSITION RANGE.

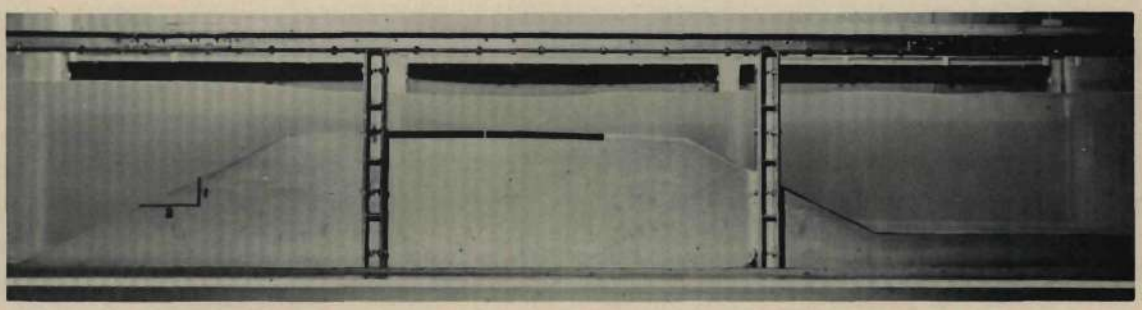

(b) INCIPIENT SUBMERGENCE, SURFACE FLOW.

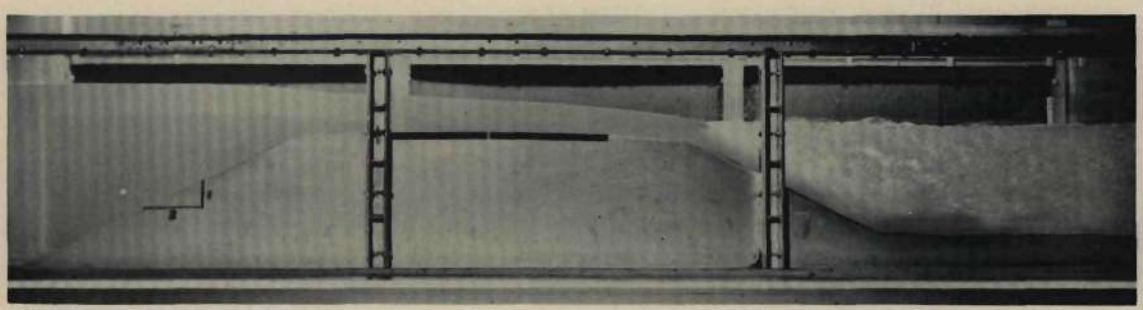

(c) FREE (PLUNGING) FLOW AT THE LOWER LIMIT OF THE TRANSITION RANGE.

Figure 6. Flow Over the Embankment. (Series B, q = 1.58 cfs/ft).

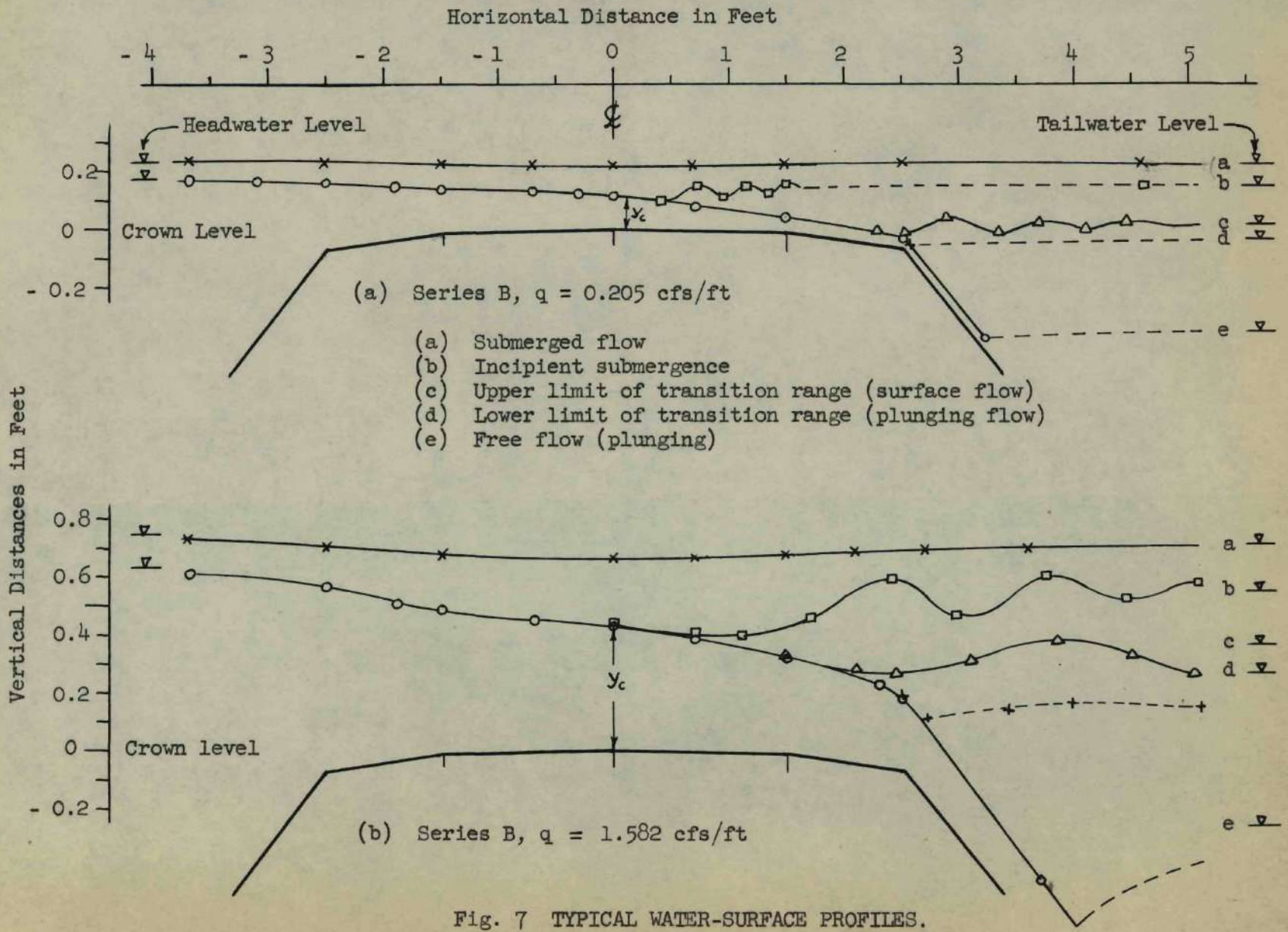

Fig. 7 TYPICAL WATER-SURFACE PROFILES.

(a) FREE FLOW.

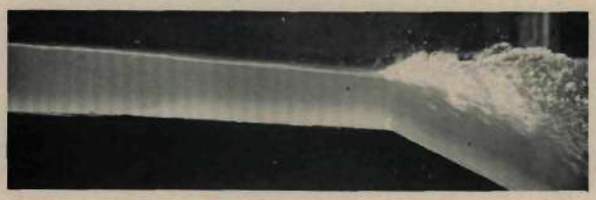

(b) FREE (PLUNGING) FLOW AT THE UPPER LIMIT OF THE TRANSITION RANGE.

(c) FREE FLOW AT THE UPPER LIMIT OF THE TRANSITION; CHANGING FROM PLUNGING TO SURFACE FLOW.

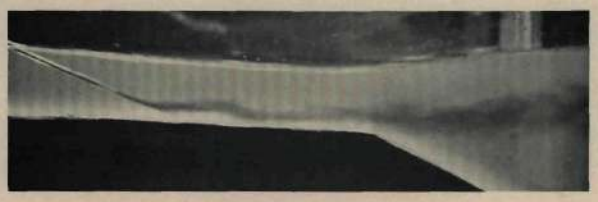

(d) FREE (SURFACE) FLOW AT THE UPPER LIMIT OF THE TRANSITION RANGE.

(e) FREE (SURFACE) FLOW, BETWEEN THE UPPER LIMIT OF THE TRANSITION AND INCIPIENT SUBMERGENCE.

(f) INCIPIENT SUBMERGENCE.

Figure 8. Changing Flow Pattern With Rising Tailwater. (Series B, q = 1.00 cfs/ft).

(a) SUBMERGED FLOW, $t/h = 0.94$.

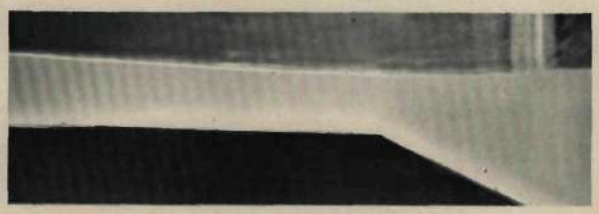

(b) FREE (SURFACE) FLOW AT THE LOWER LIMIT OF THE TRANSITION RANGE.

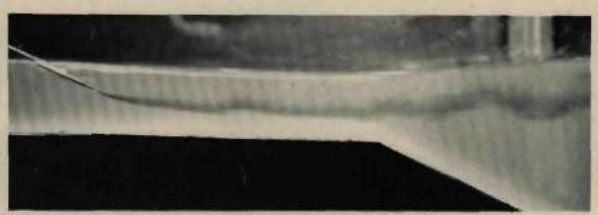

(c) SAME AS (b), WITH DYE INJECTION.

(d) FREE FLOW AT THE LOWER LIMIT OF THE TRANSITION; CHANGING FROM SURFACE TO PLUNGING FLOW.

(e) FREE (PLUNGING) FLOW AT THE LOWER LIMIT OF THE TRANSITION RANGE.

Figure 9. Changing Flow Pattern With Falling Tailwater. (Series B, q = 1.00 cfs/ft).

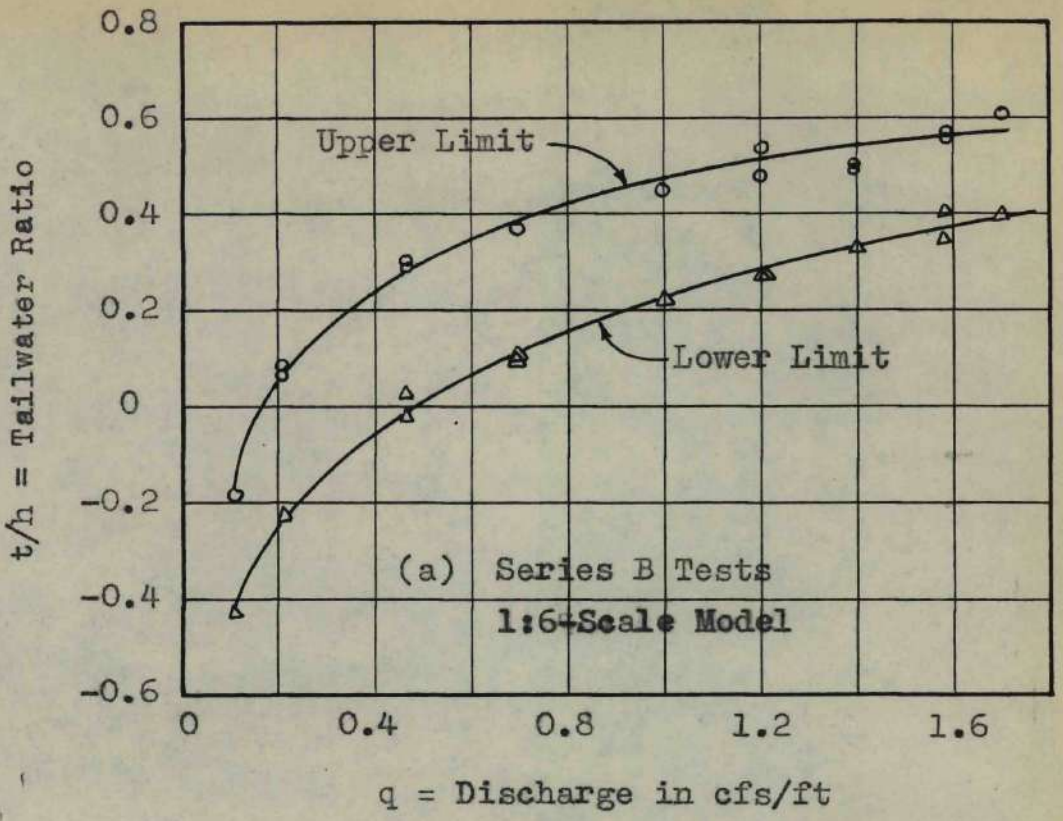

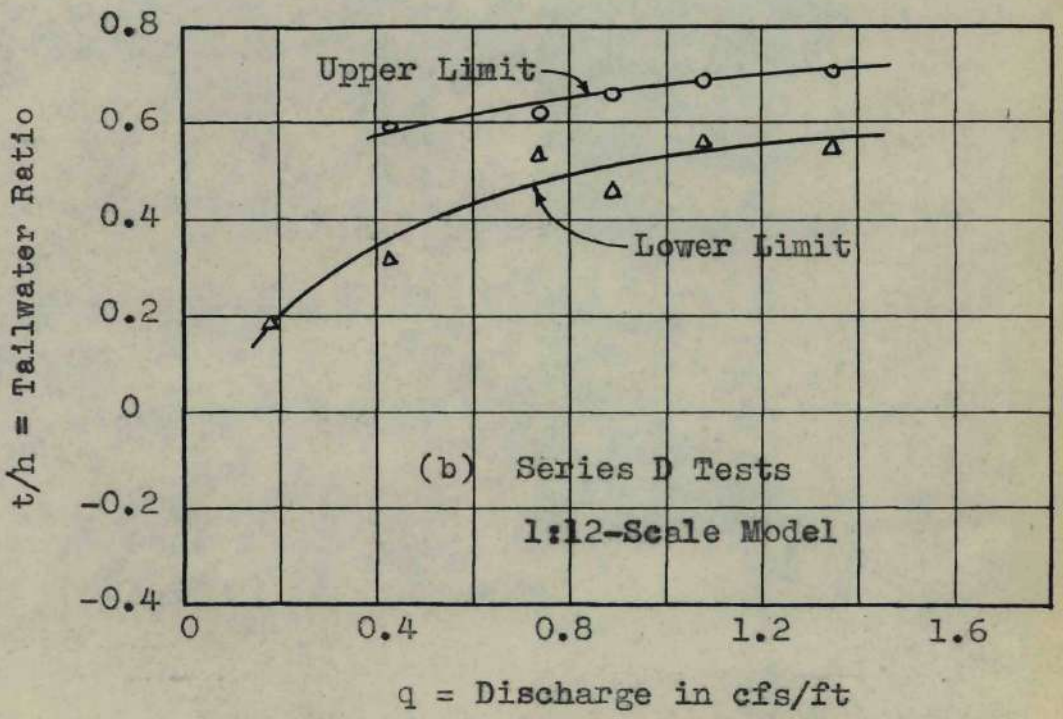

Fig. 10. DEFINITION OF FREE-FLOW TRANSITION RANGE.

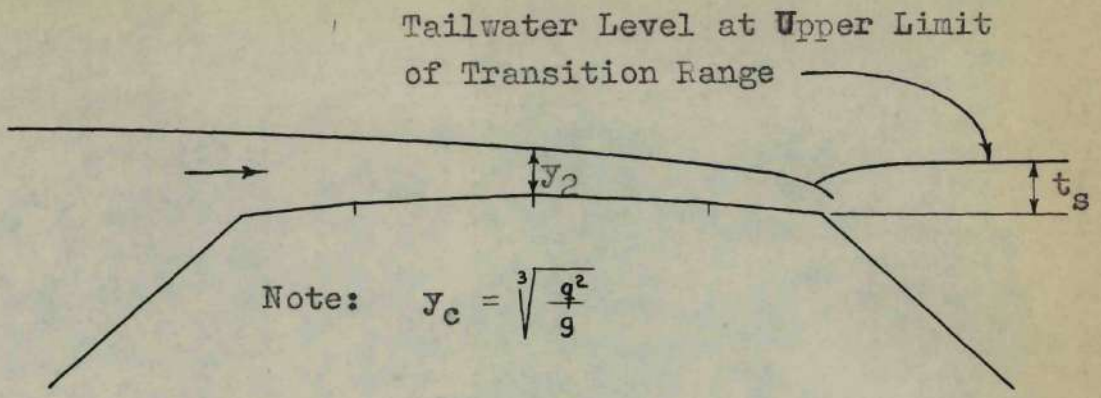

(a) Definition Sketch for Figures 11 and 12.

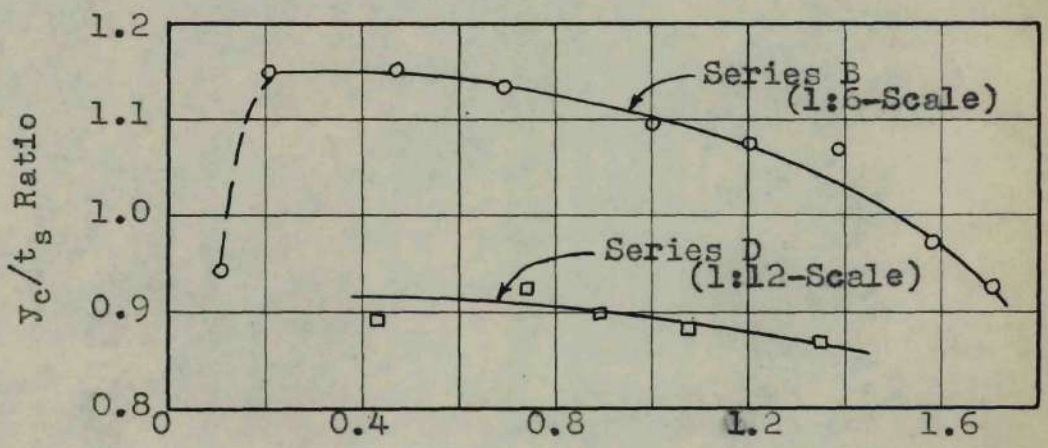

(b) Results of Test Series B and D.

Fig. 11. TAILWATER LEVEL AT UPPER LIMIT OF TRANSITION RANGE.

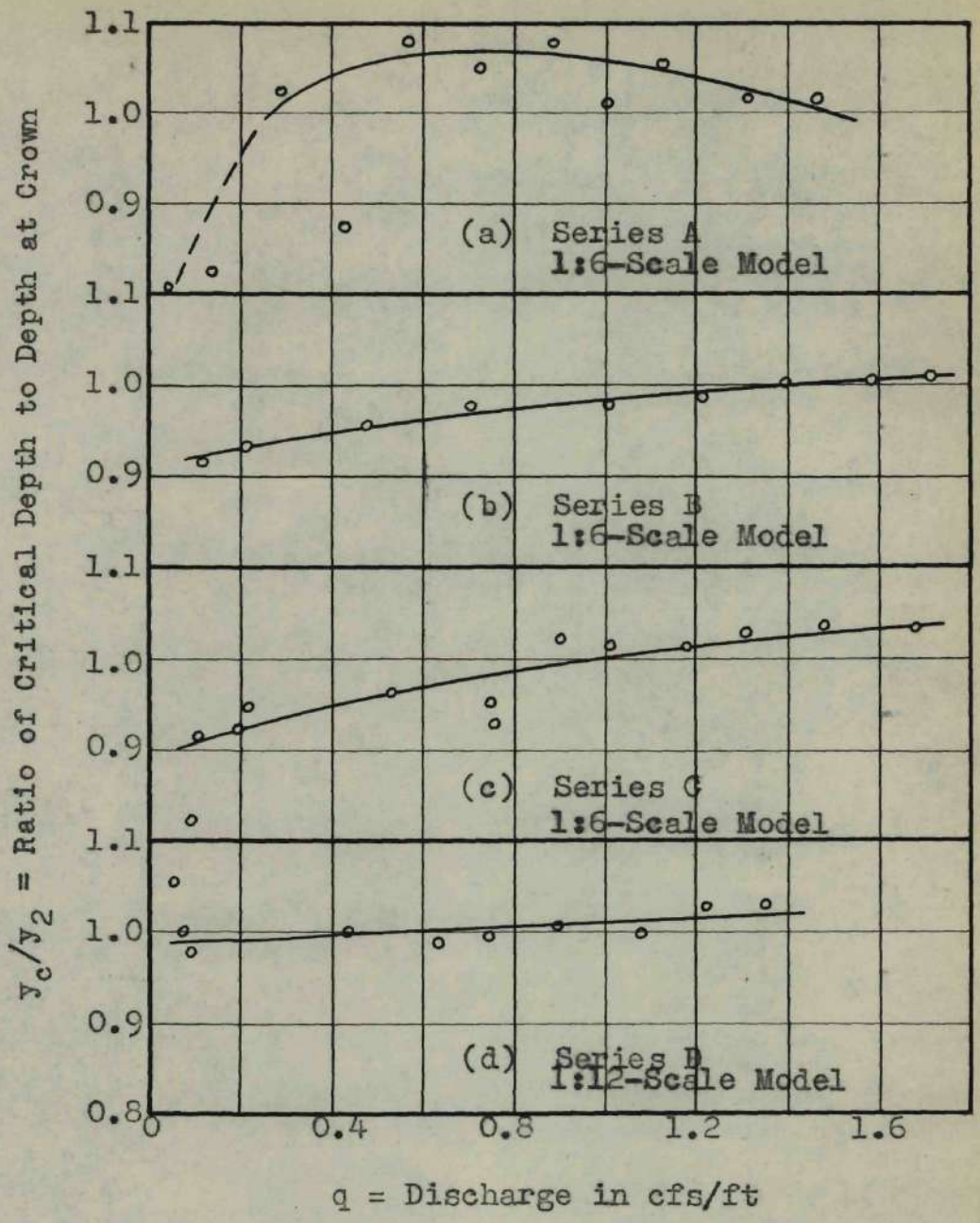

Fig. 12. RATIO OF CRITICAL DEPTH TO DEPTH AT CROWN.

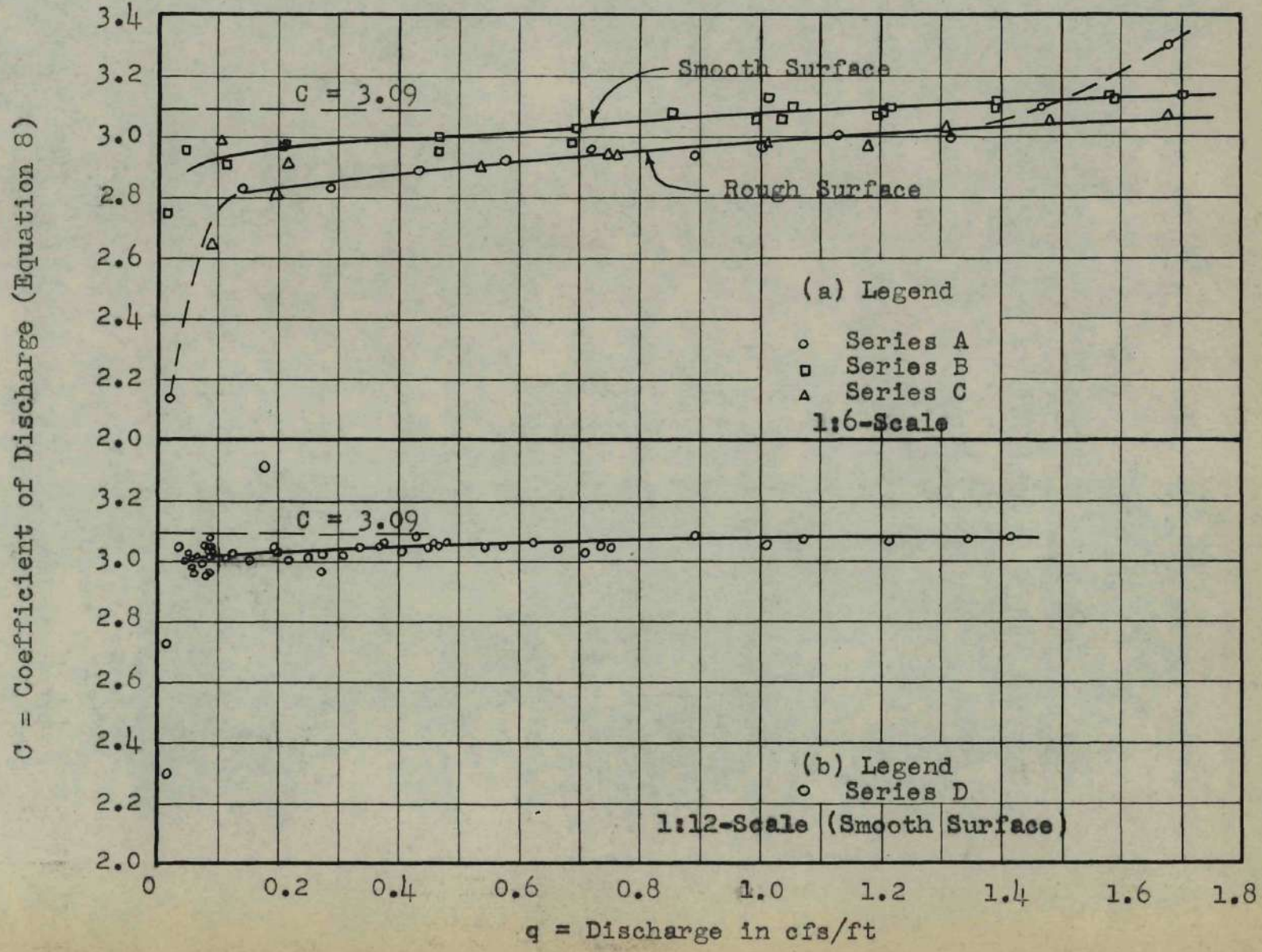

Fig. 13. COEFFICIENTS OF FREE DISCHARGE, SERIES A TO D, INCLUSIVE.

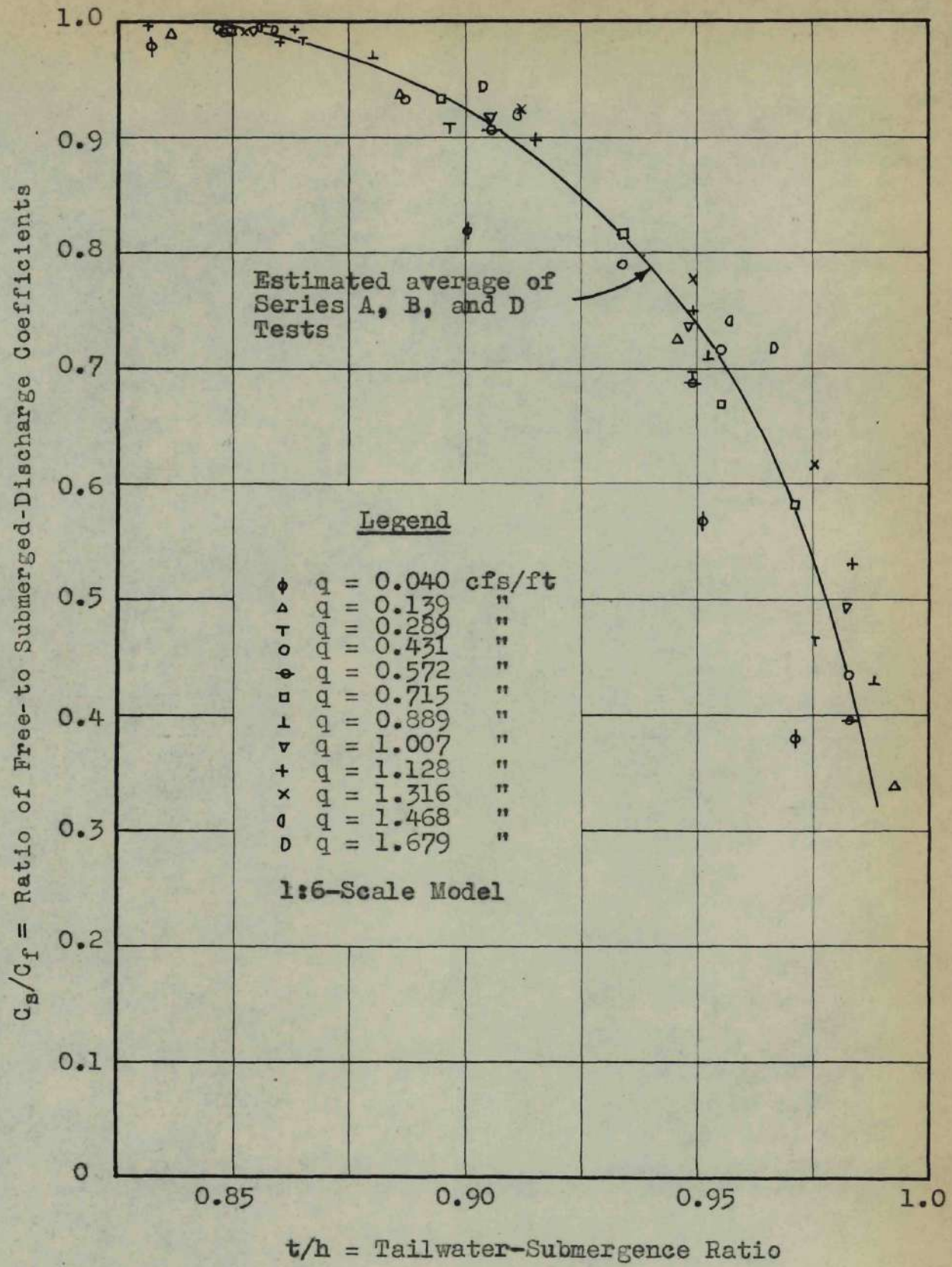

Fig. 14. SUBMERGED DISCHARGE, SERIES A.

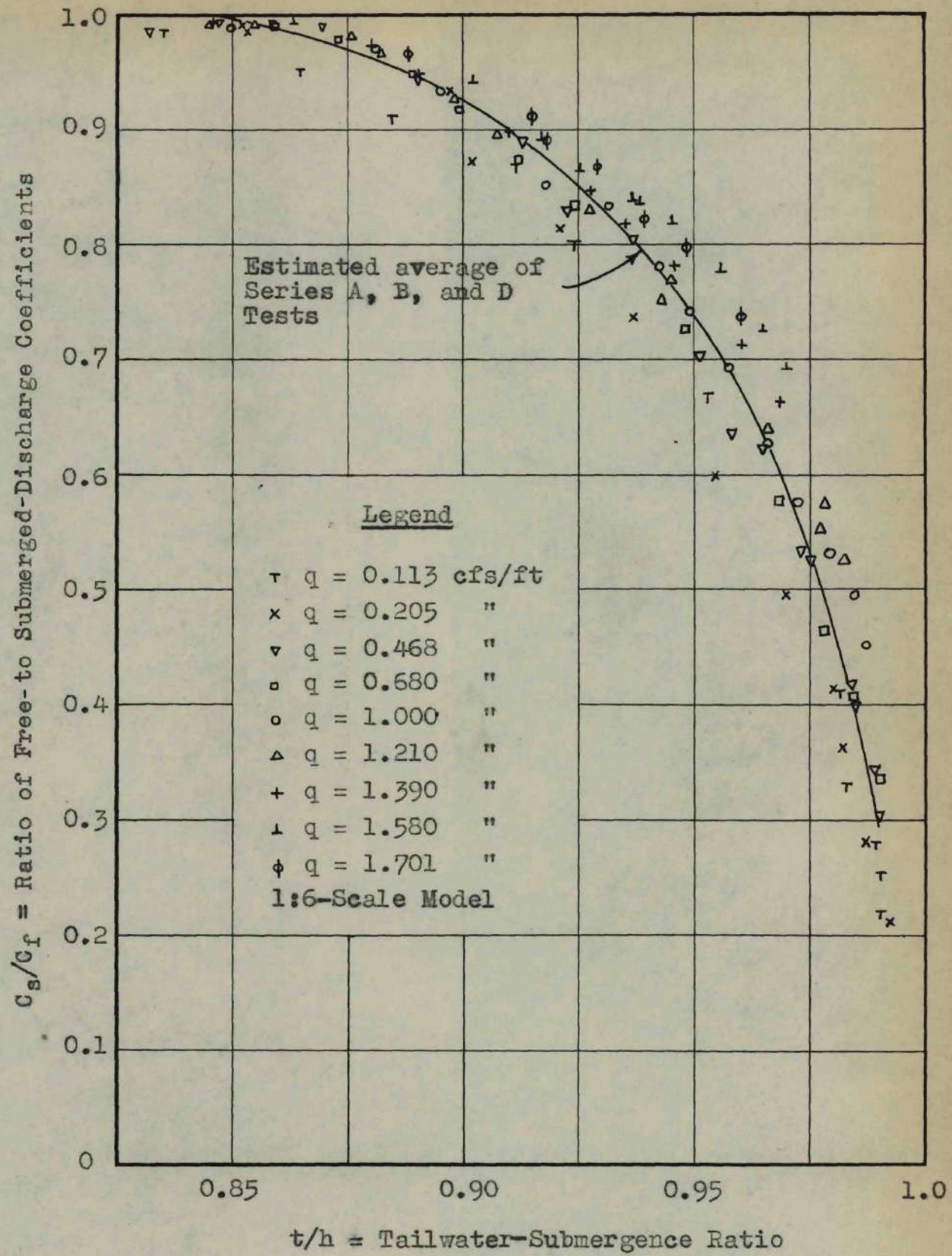

Fig. 15. SUBMERGED DISCHARGE, SERIES B.

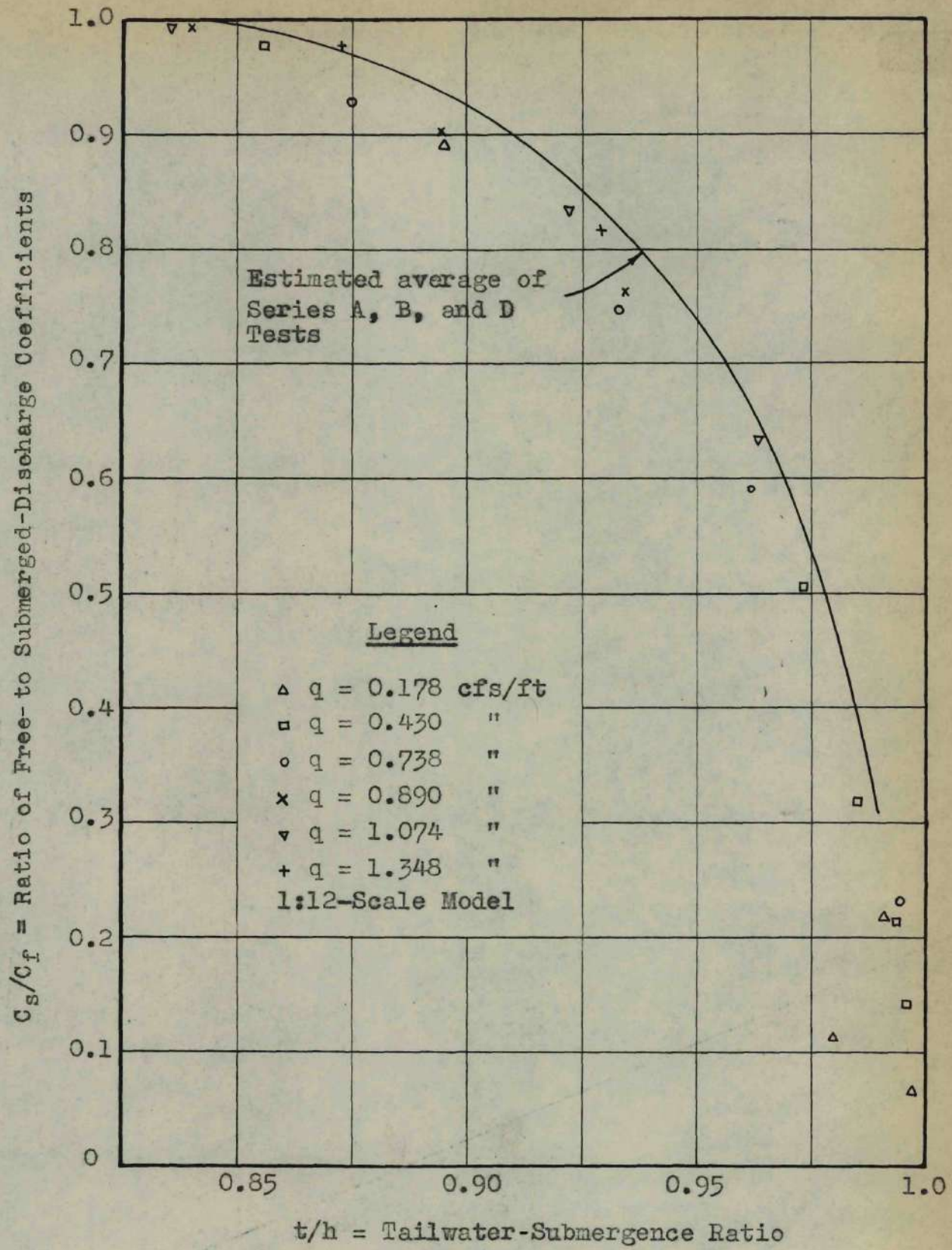

Fig. 16. SUBMERGED DISCHARGE, SERIES D.

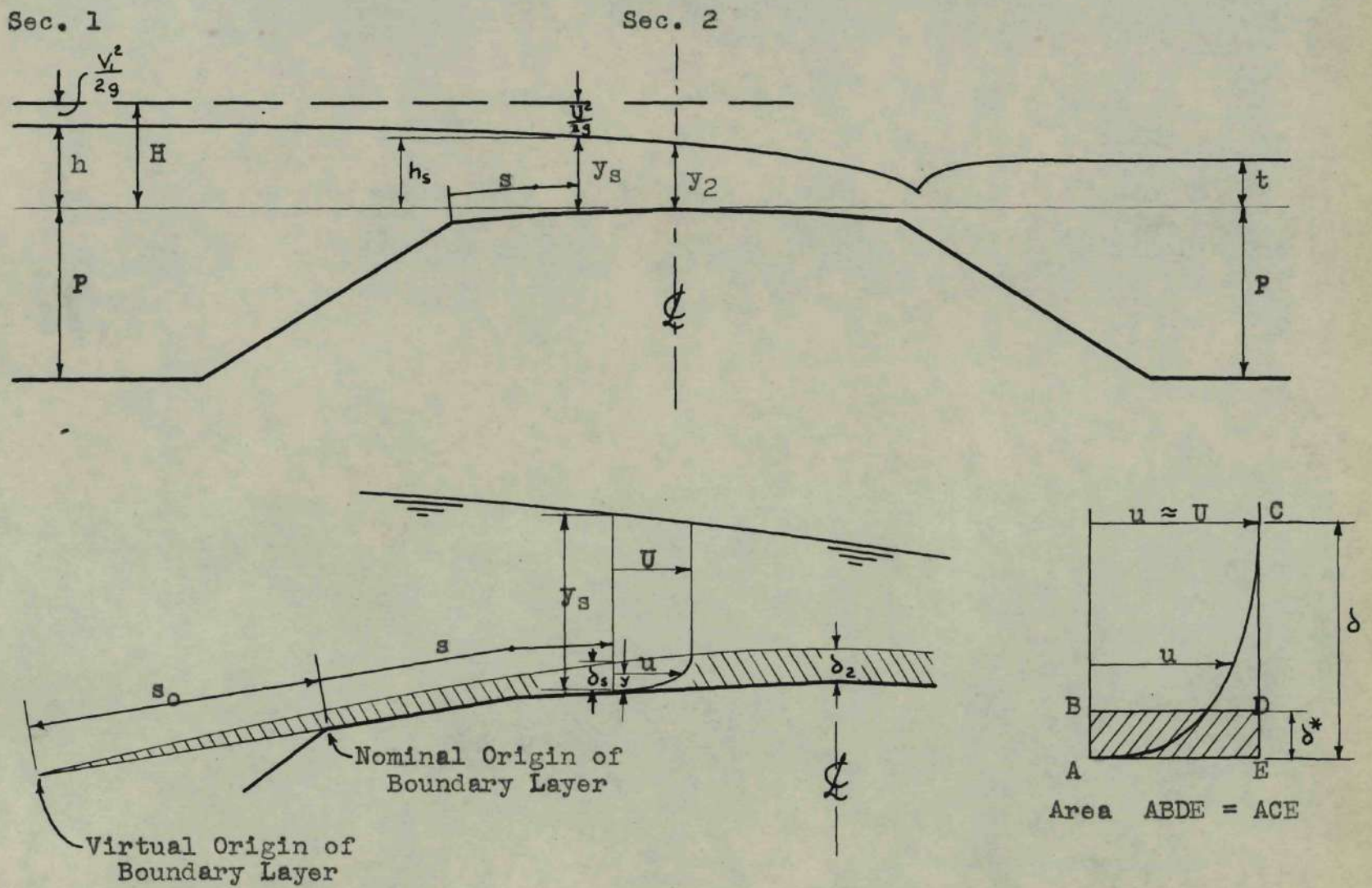

Fig. 17. DEFINITION SKETCHES FOR DISCHARGE AND BOUNDARY LAYER EQUATIONS.

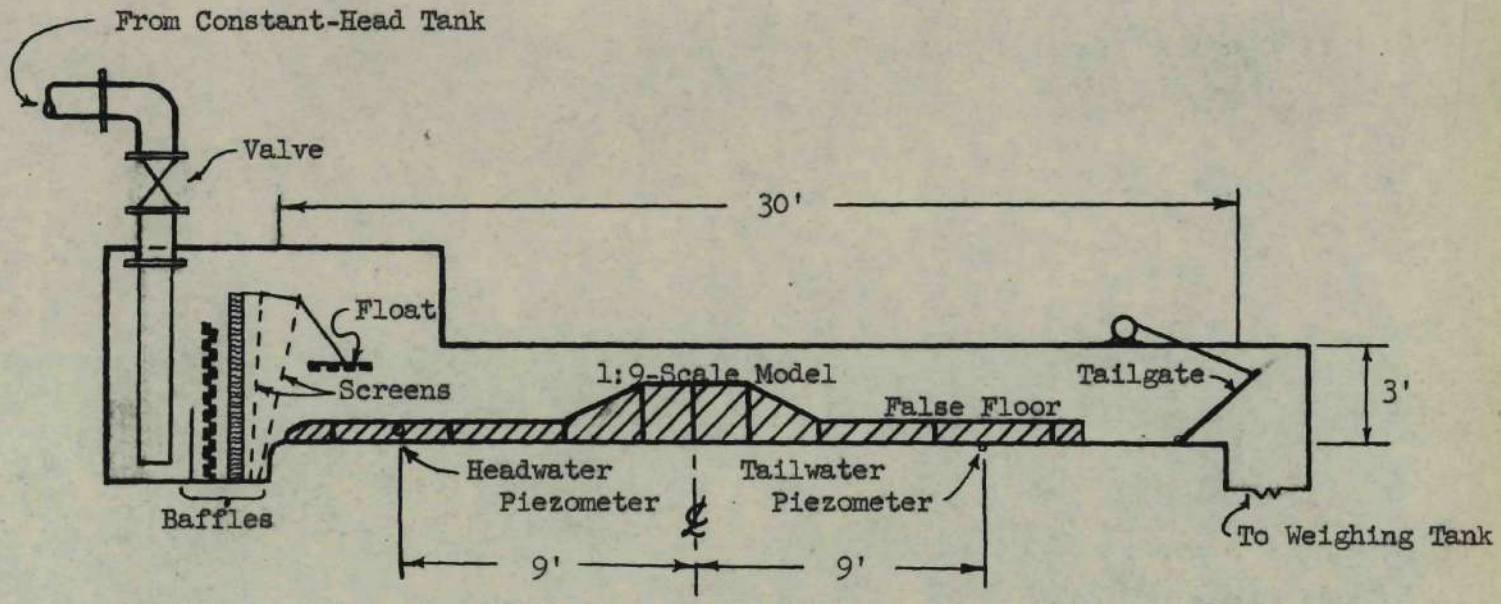

Fig. 18. GENERAL ARRANGEMENT OF EXPERIMENTAL EQUIPMENT.

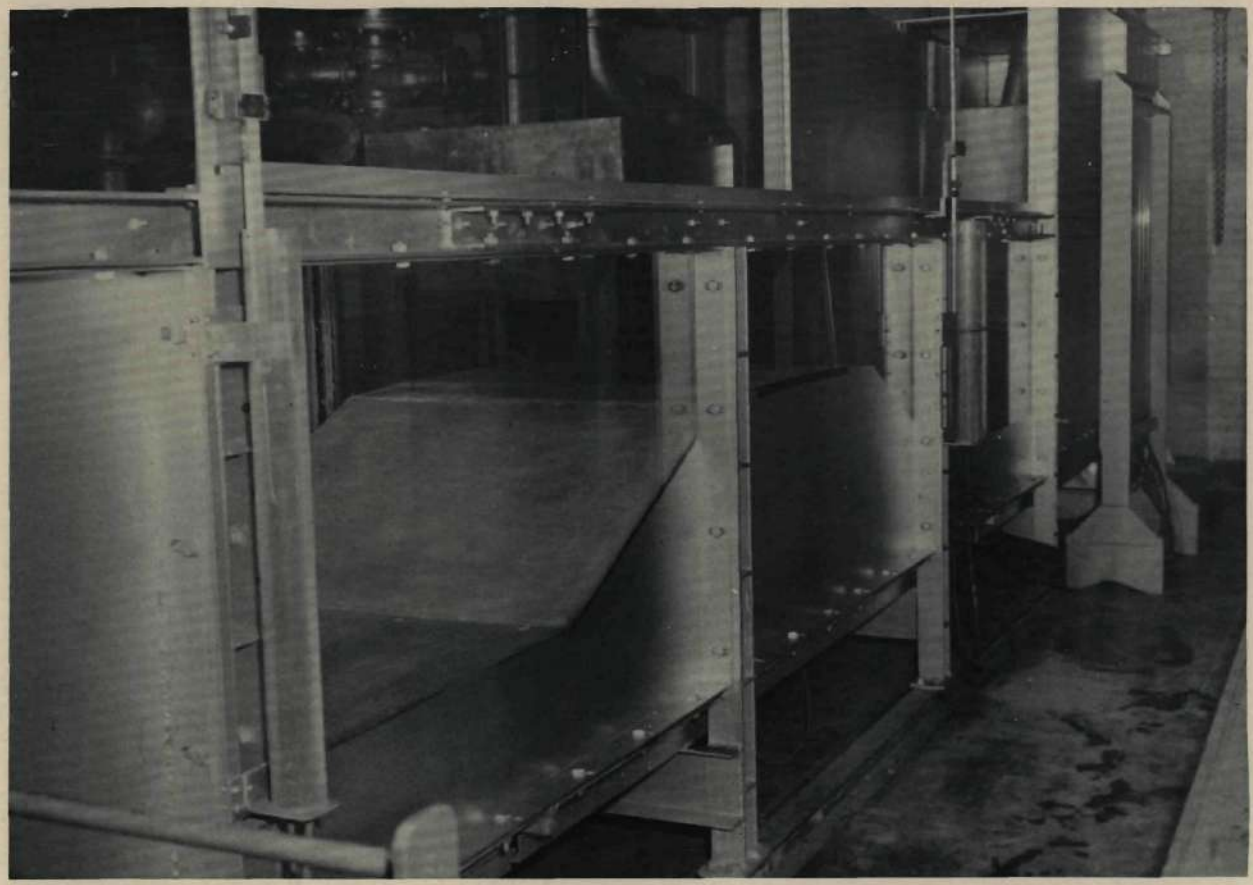

Figure 19. Looking Upstream at the 1:9-Scale Model.

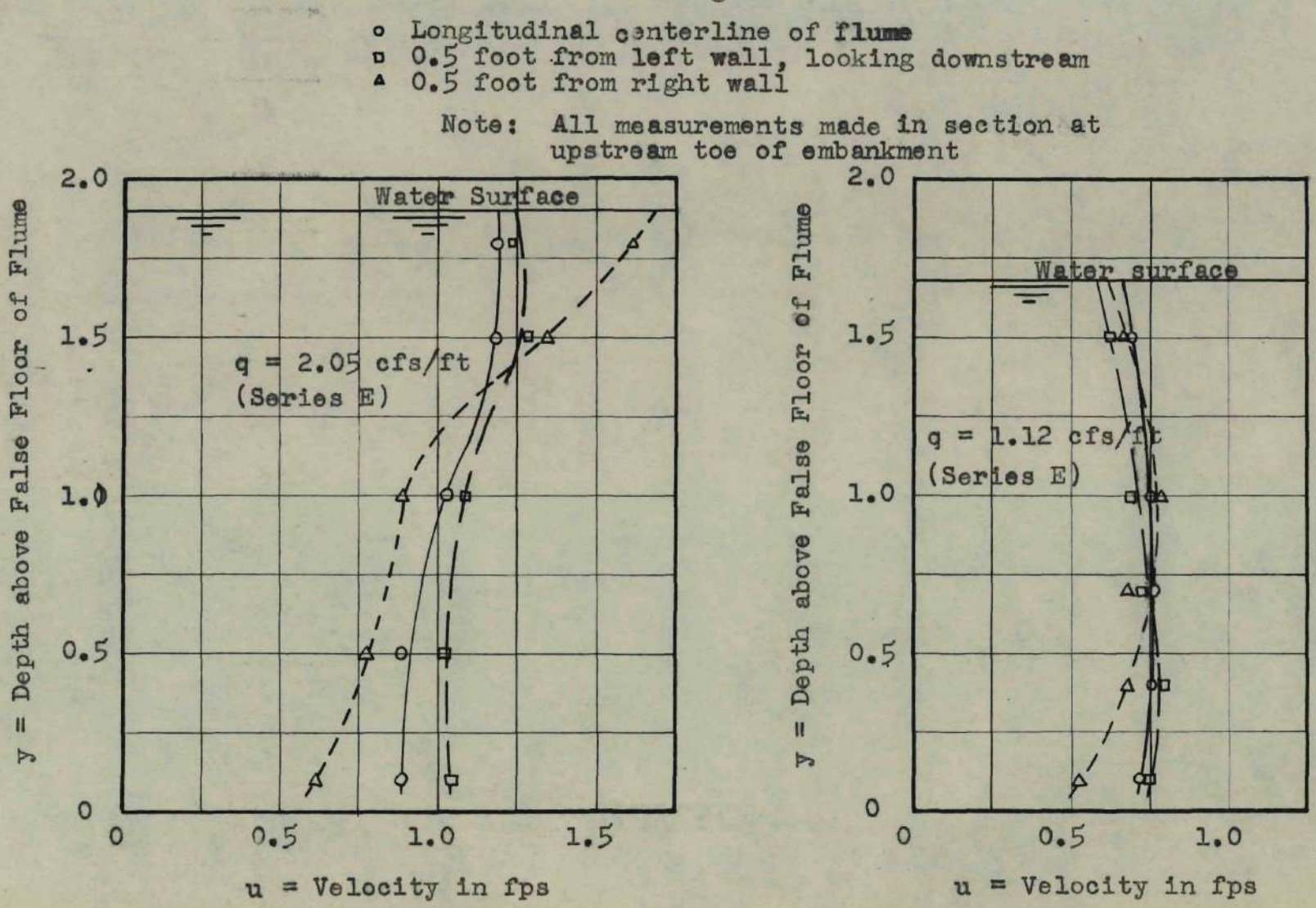

Fig. 20. VELOCITY DISTRIBUTION IN THE FLUME.

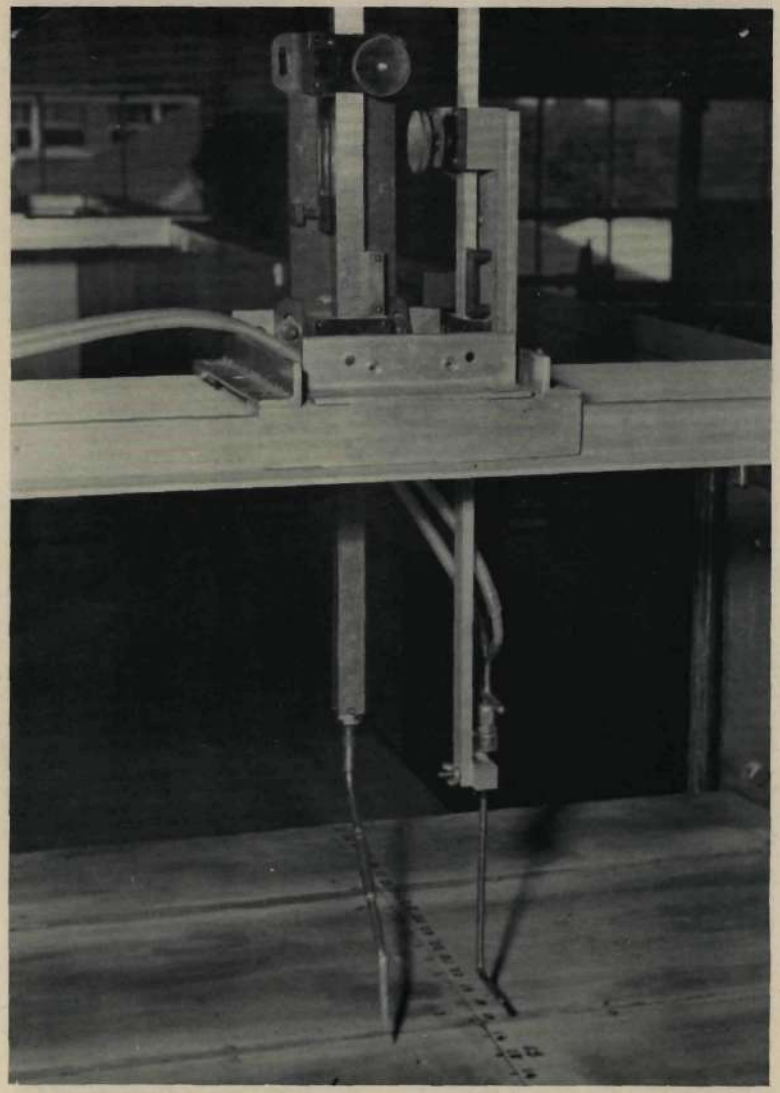

Figure 21. Point Gage and Pitot-Static Tube.

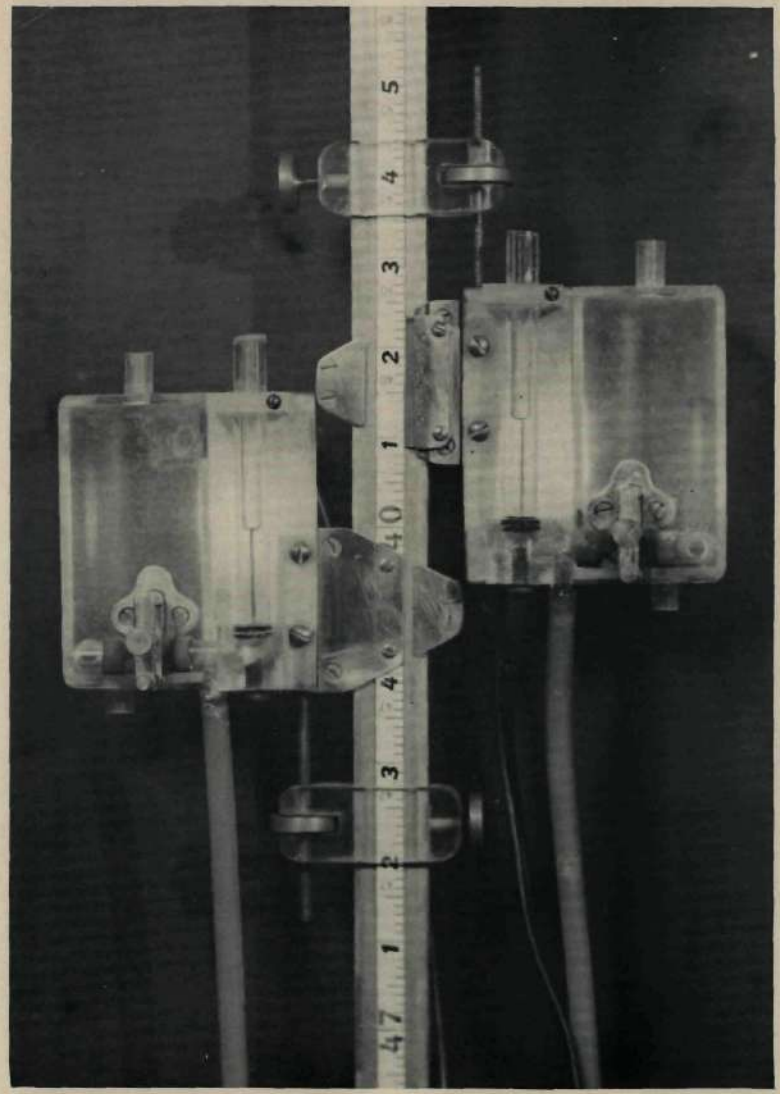

Figure 22. Manometer for the Pitot-Static Tube.

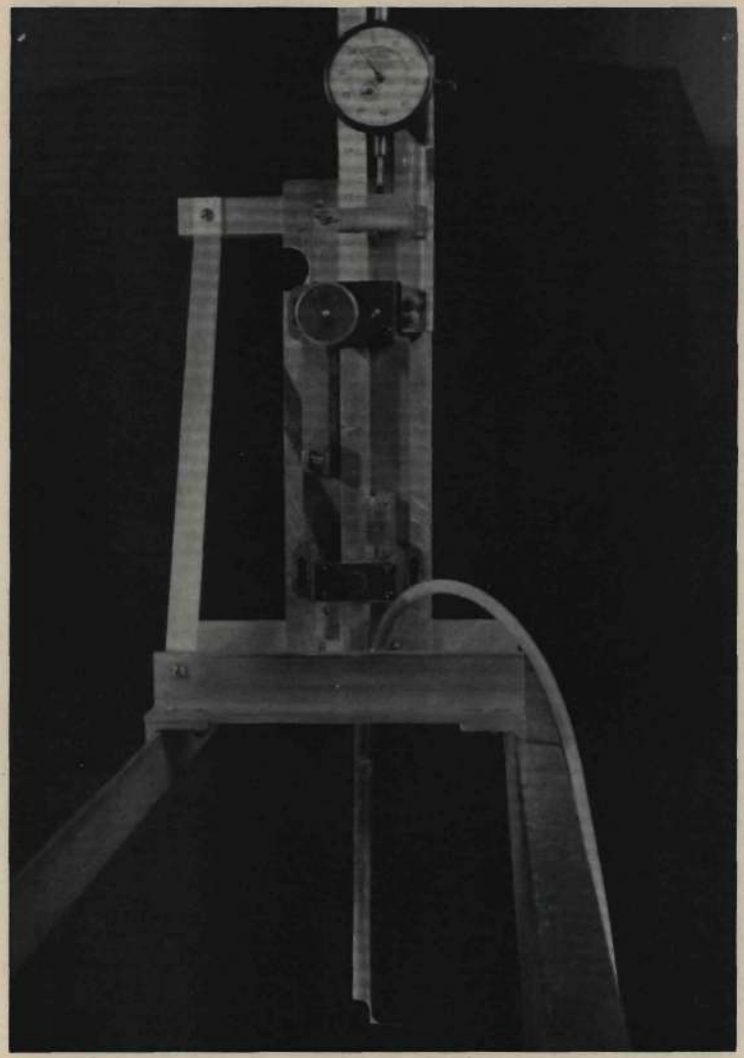

Figure 23. Stagnation Tube for Boundary Layer Measurements.

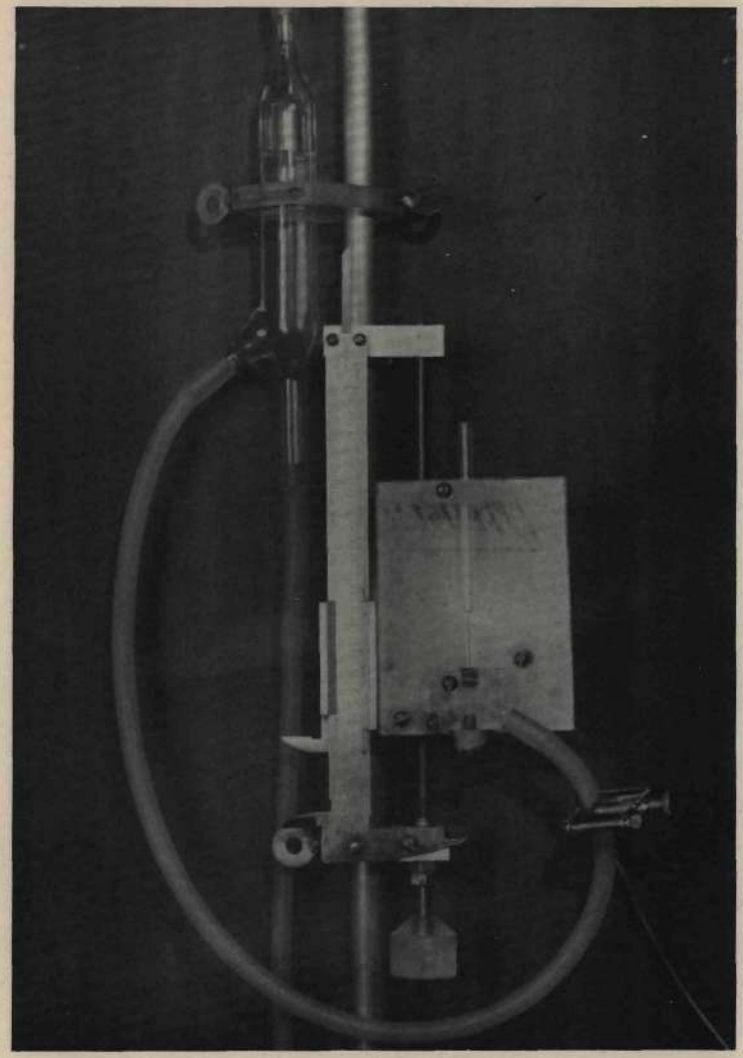

Figure 24. Manometer for Stagnation Tube.

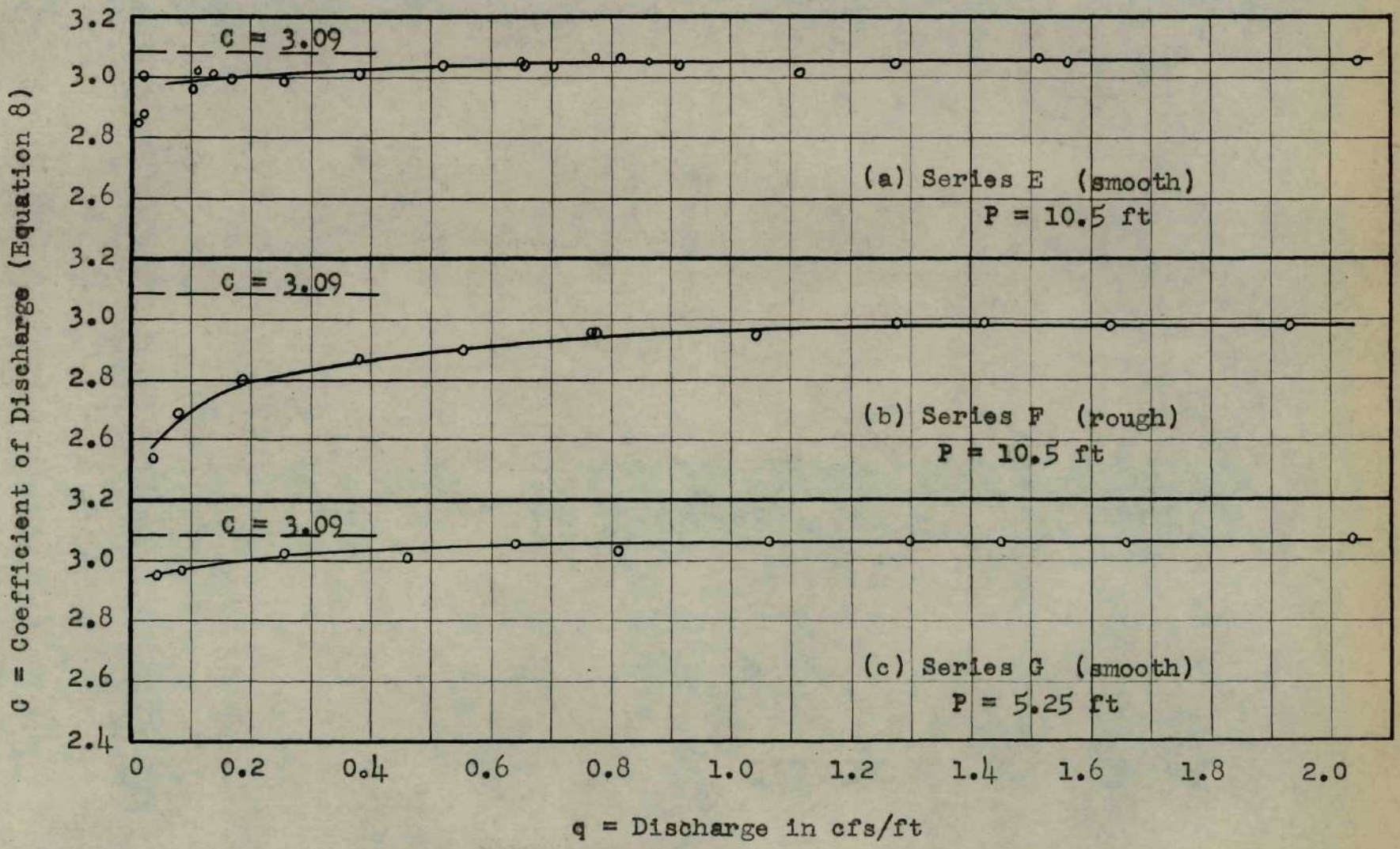

Fig. 25. COEFFICIENT OF FREE DISCHARGE, SERIES E, F AND G.

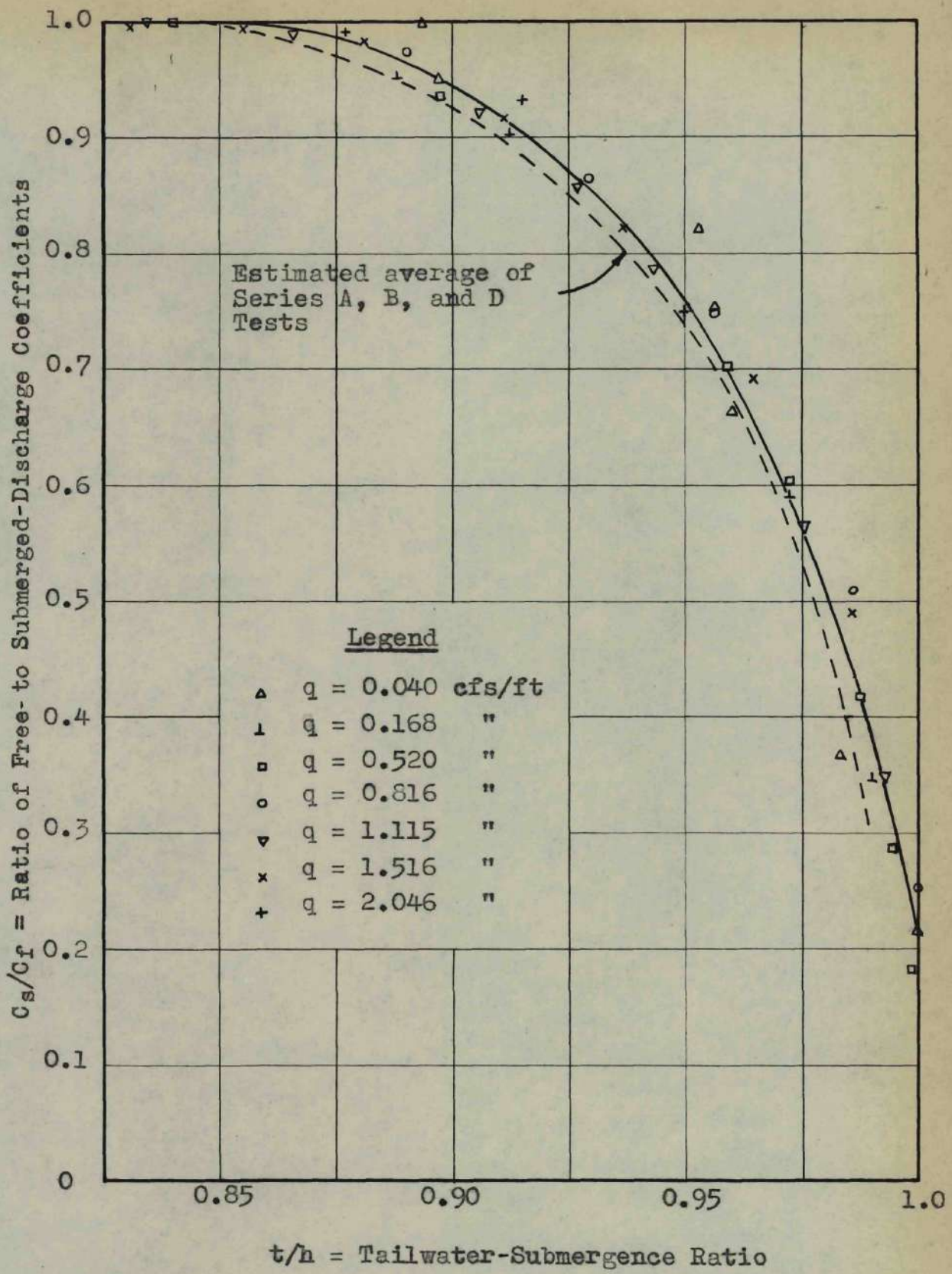

Fig. 26. SUBMERGED DISCHARGE, SERIES E.

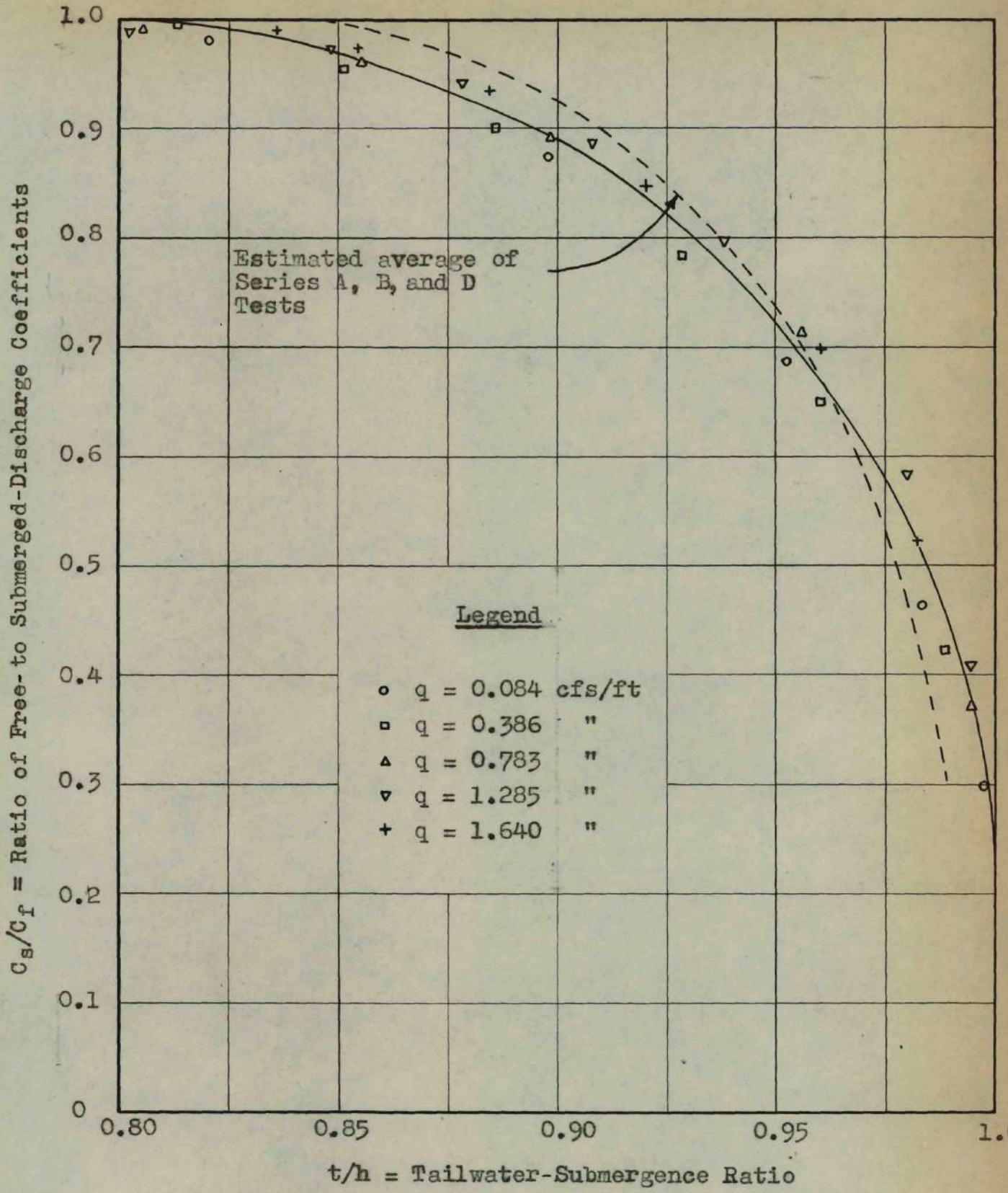

Fig. 27. SUBMERGED DISCHARGE, SERIES F.

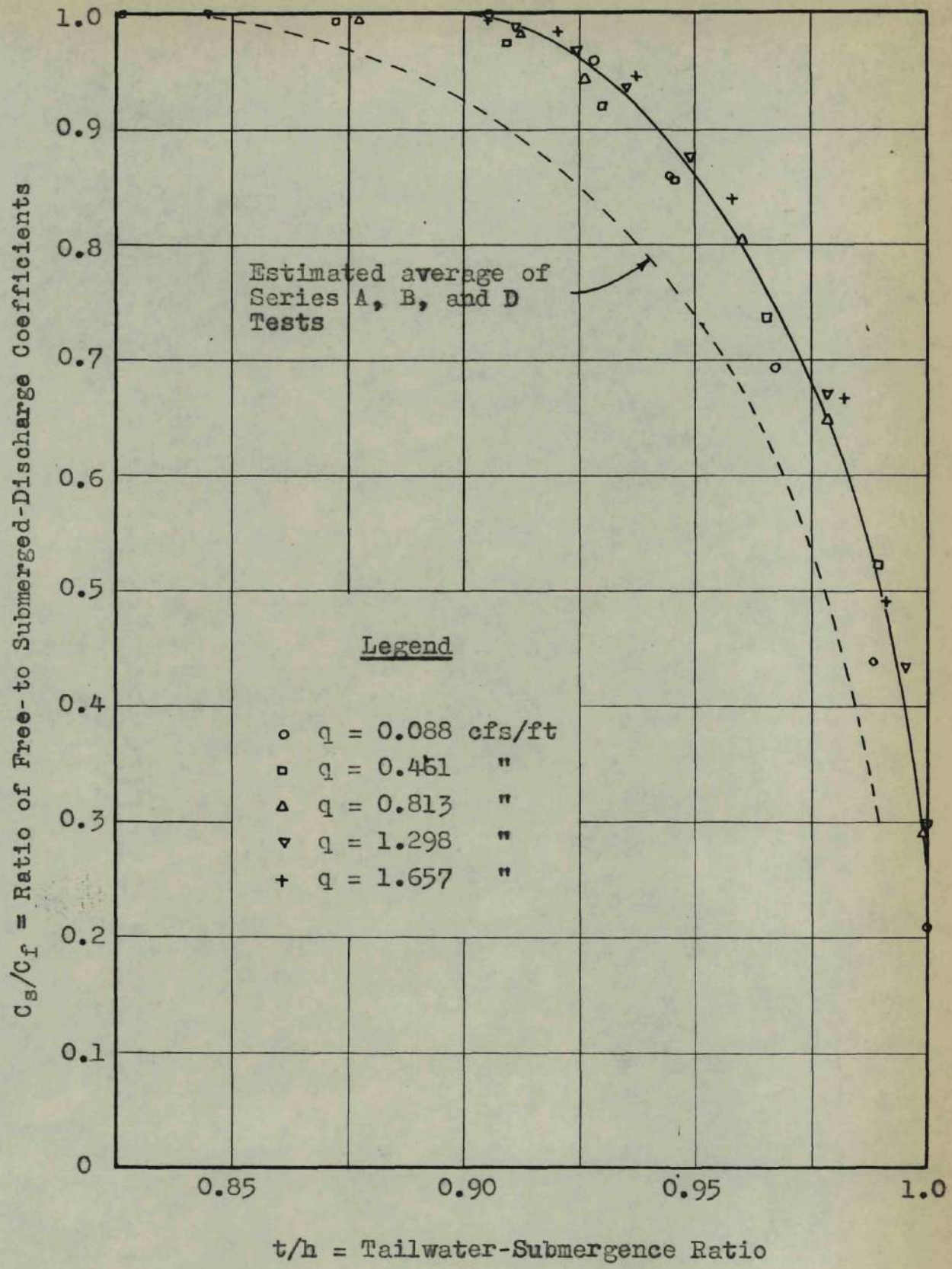

Fig. 28. SUBMERGED DISCHARGE, SERIES G.

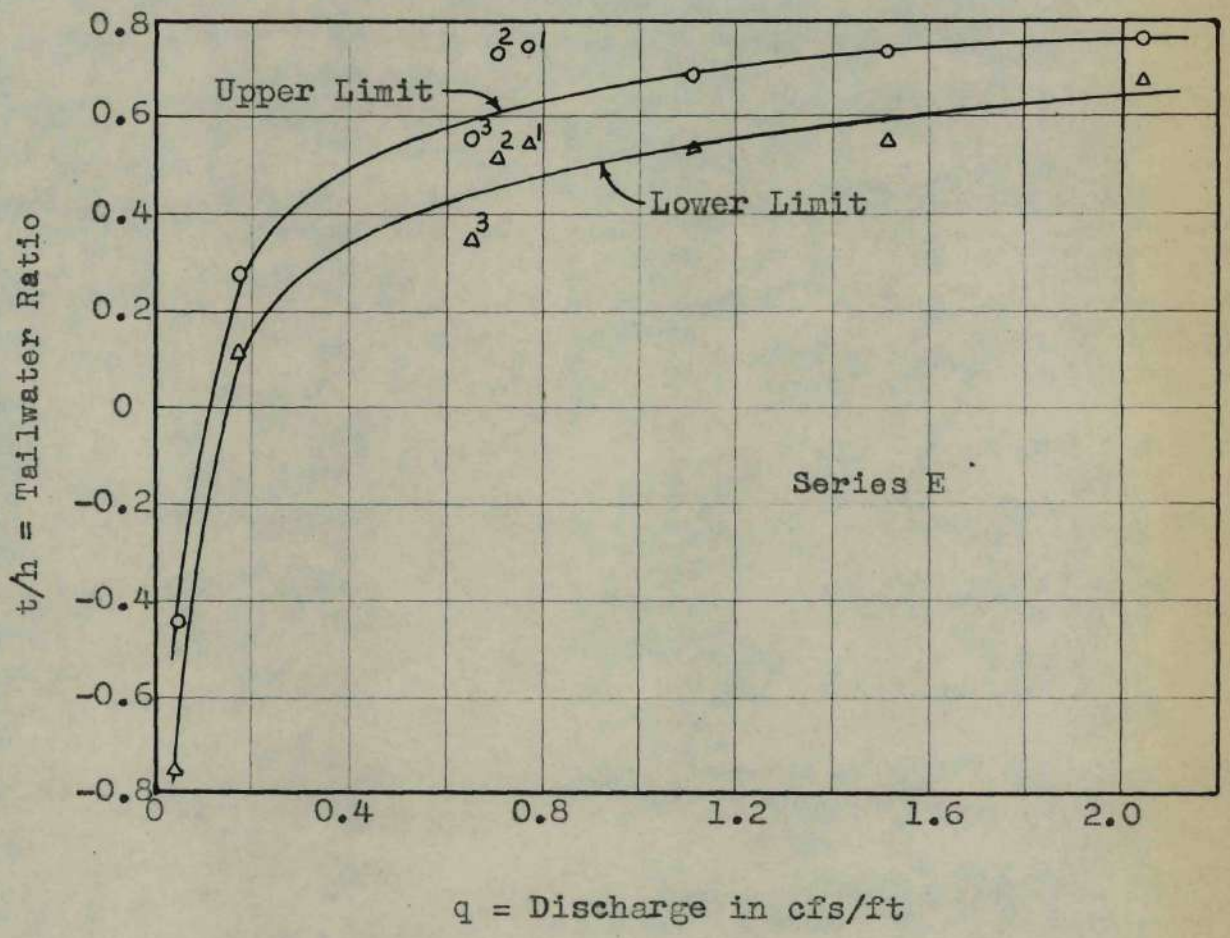

Fig. 29. DEFINITION OF FREE-FLOW TRANSITION RANGE.

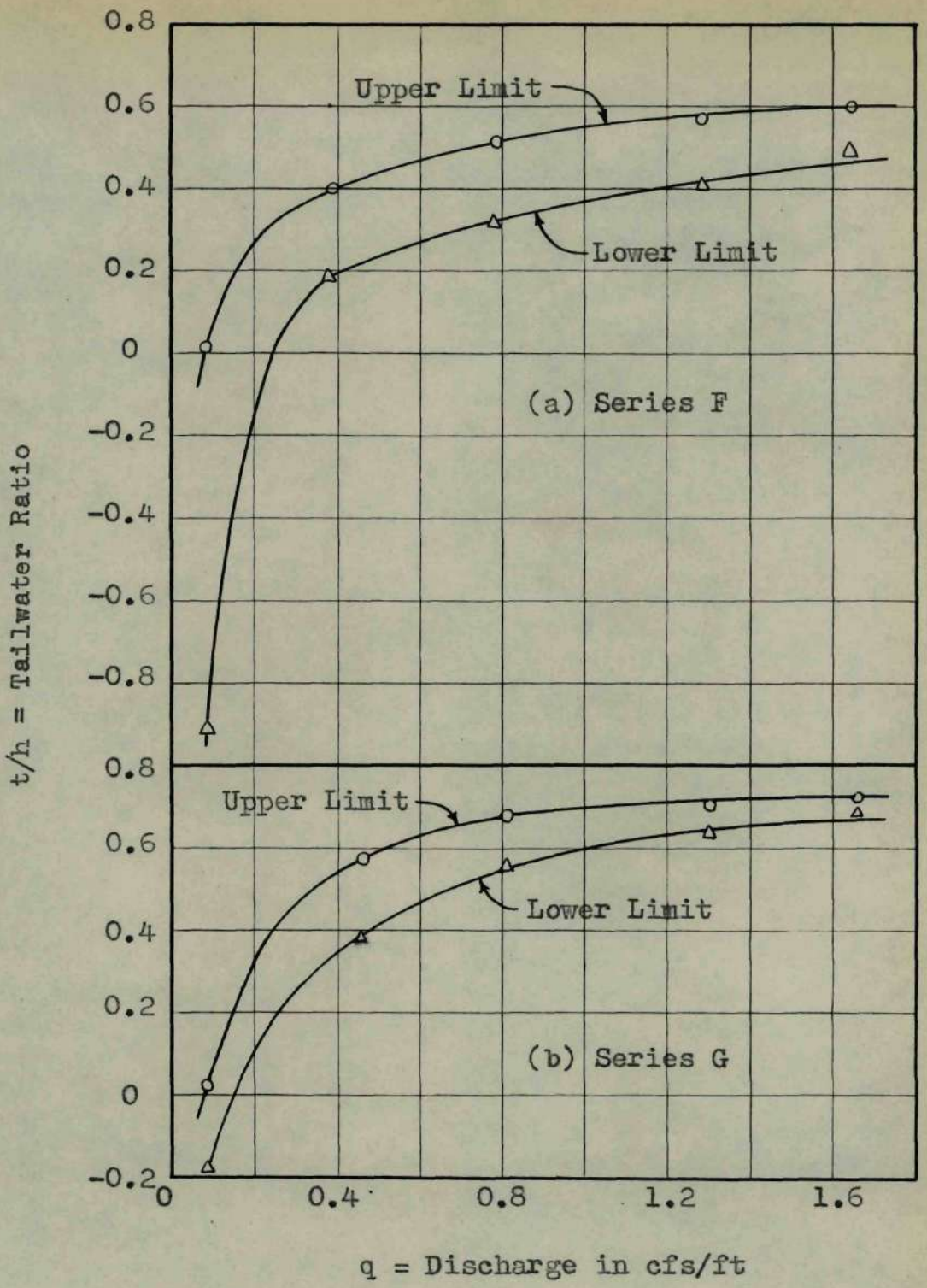

Fig. 30. DEFINITION OF FREE-FLOW TRANSITION RANGE.

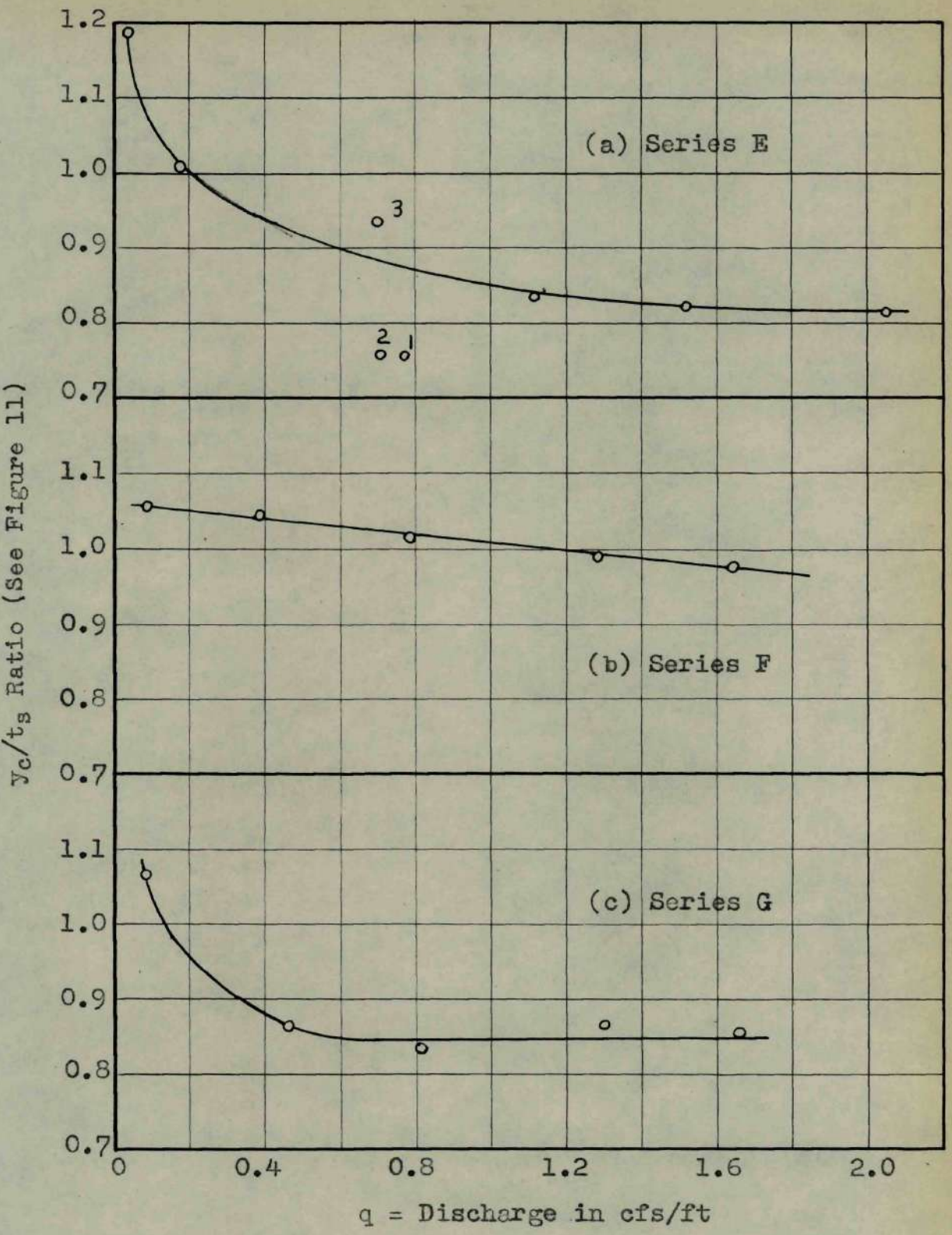

Fig. 31. TAILWATER LEVEL AT UPPER LIMIT OF TRANSITION RANGE.

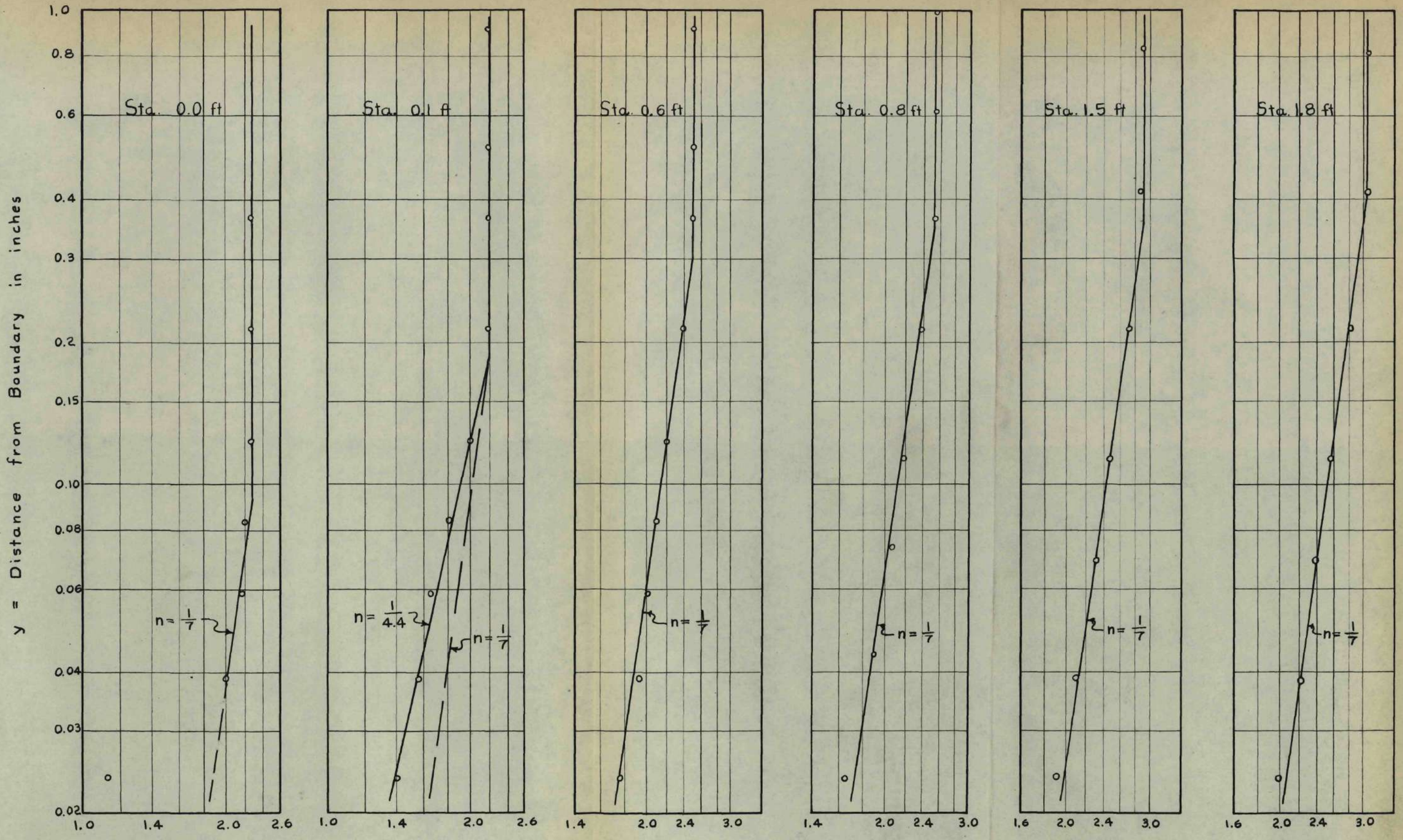

Fig. 32. VELOCITY TRAVERSES, TEST 1

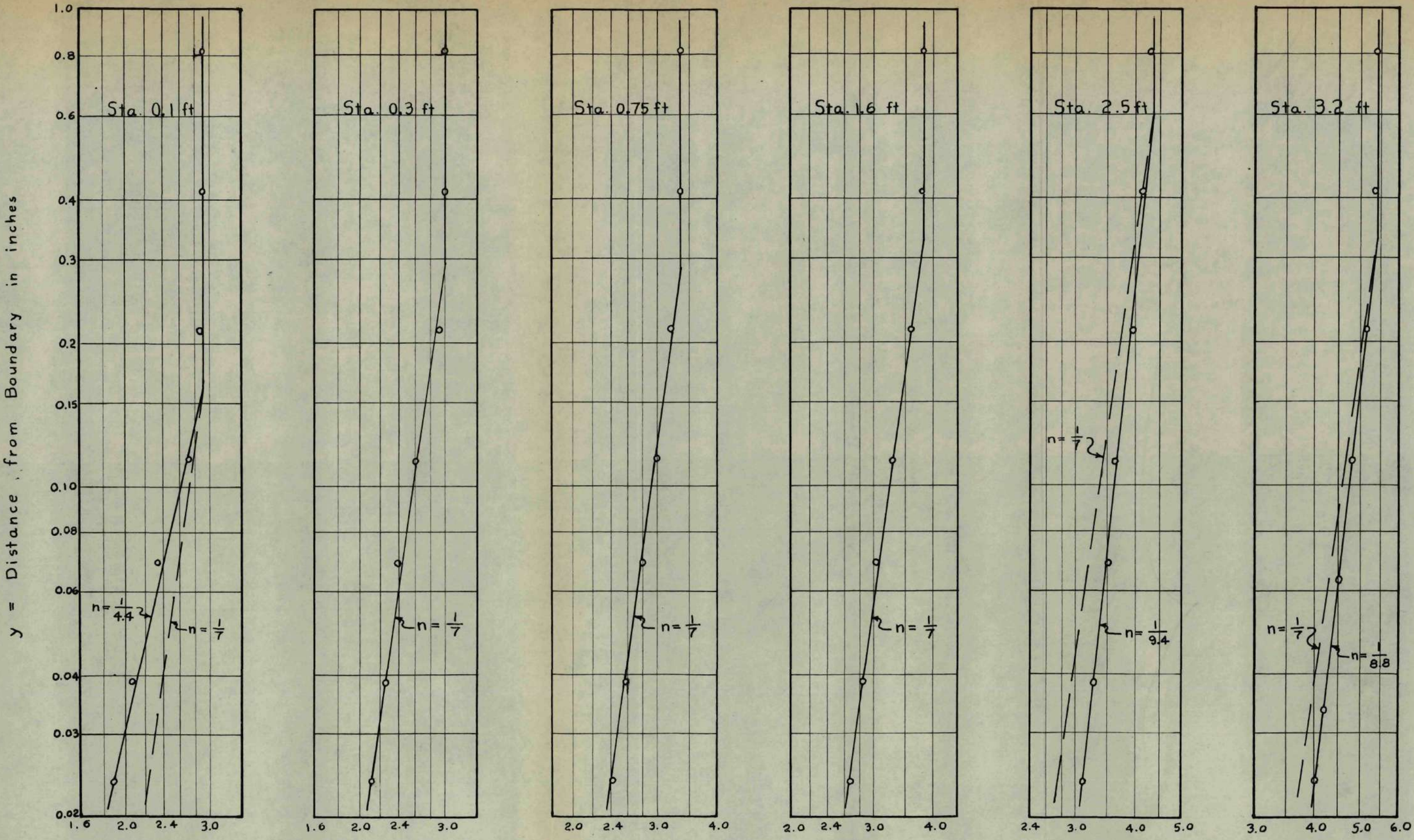

Fig. 33. VELOCITY TRAVERSES, TEST 2.

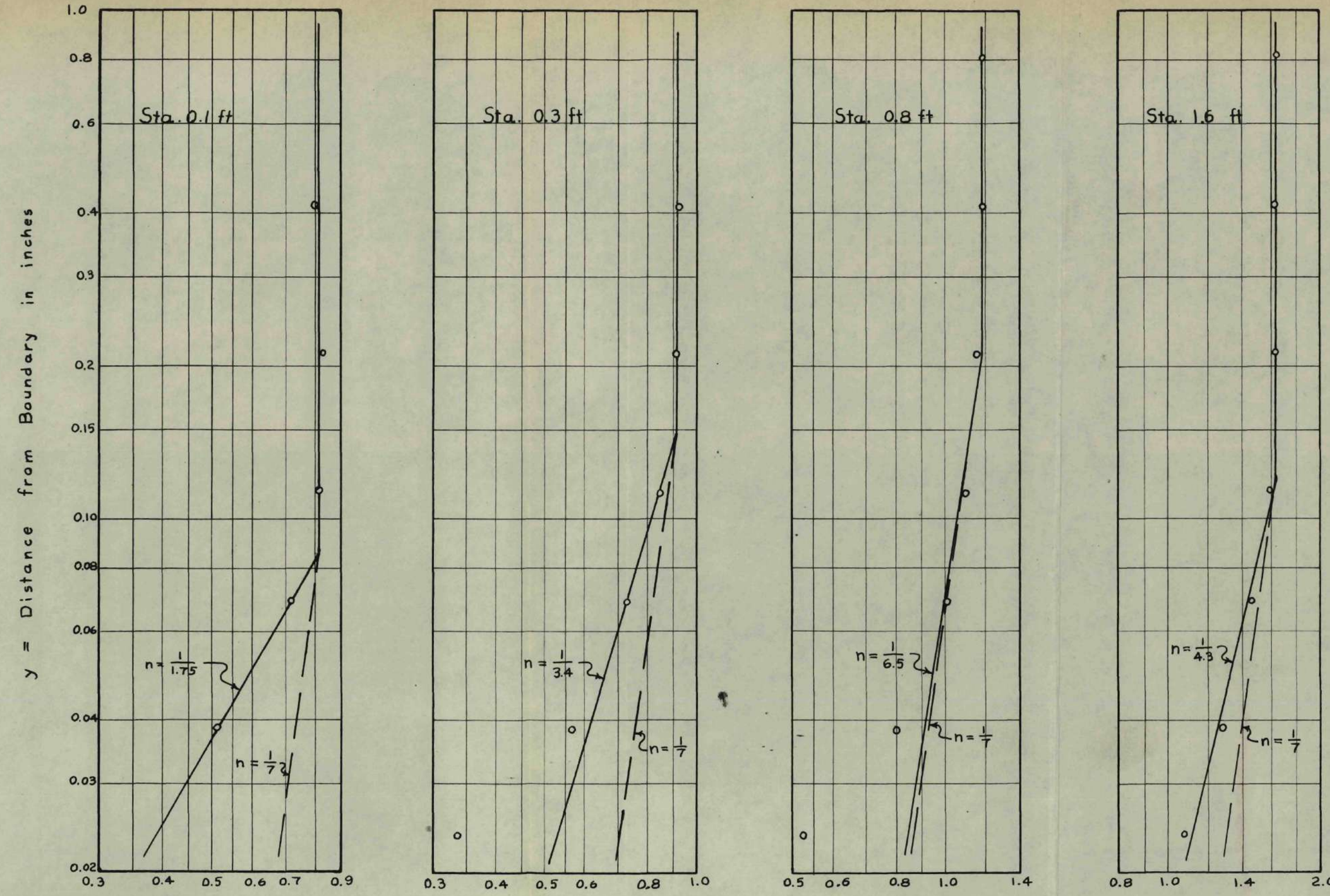

Fig. 34. VELOCITY TRAVERSES, TEST 4.

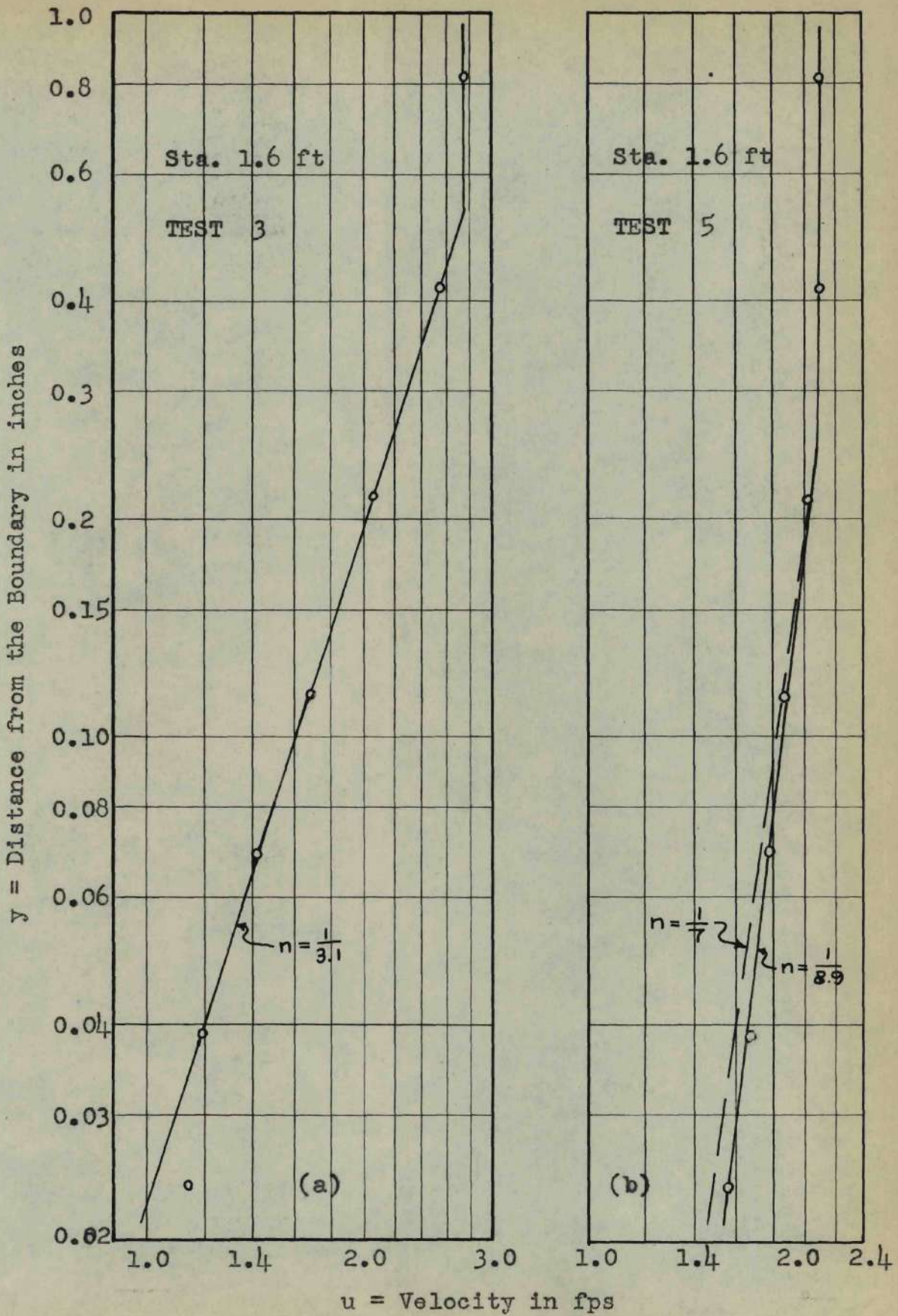

Fig. 35. VELOCITY TRAVERSES, TESTS 3 AND 5.

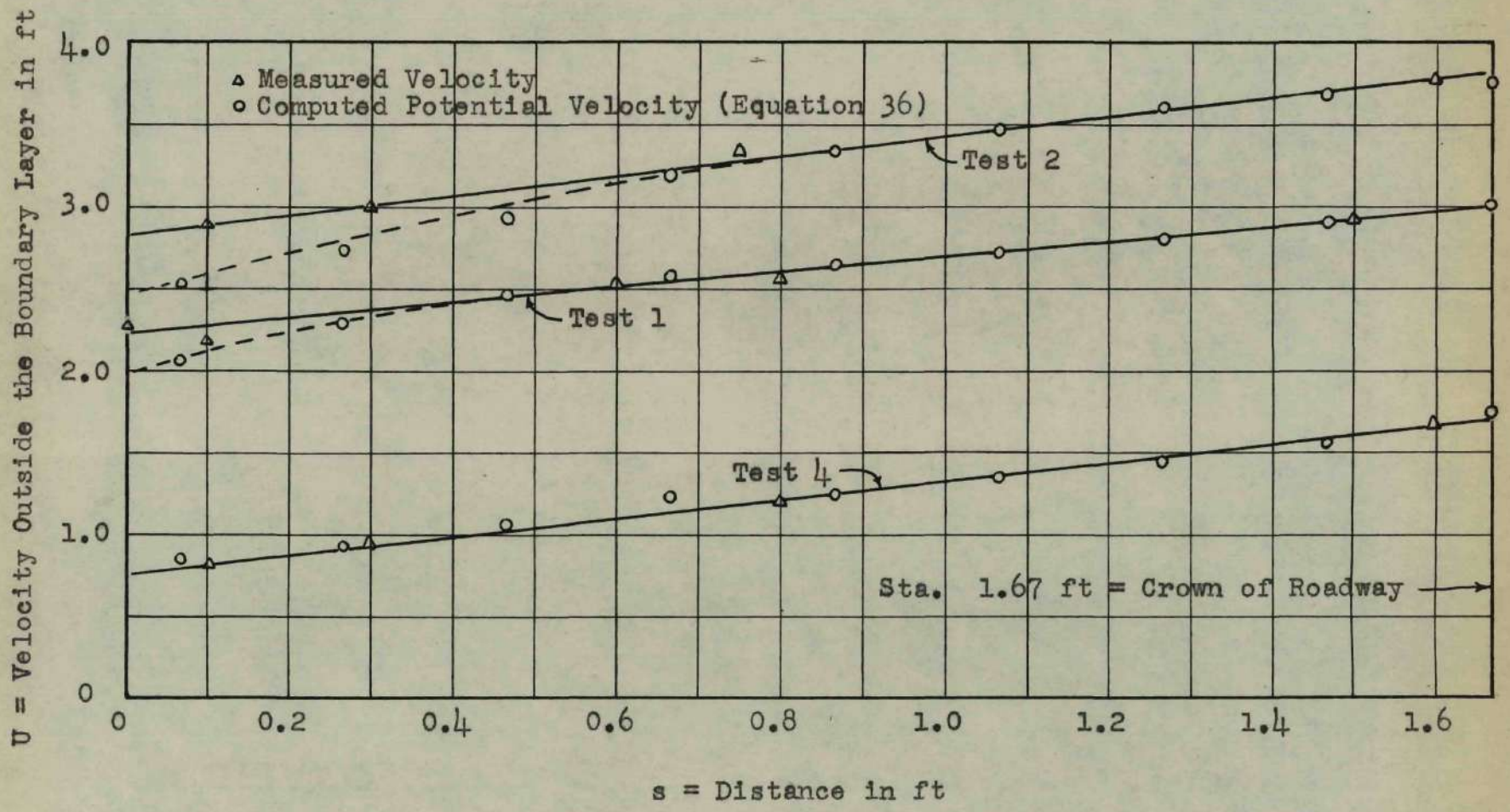

Fig. 36. VELOCITY OUTSIDE THE BOUNDARY LAYER, TESTS 1, 2 AND 4.

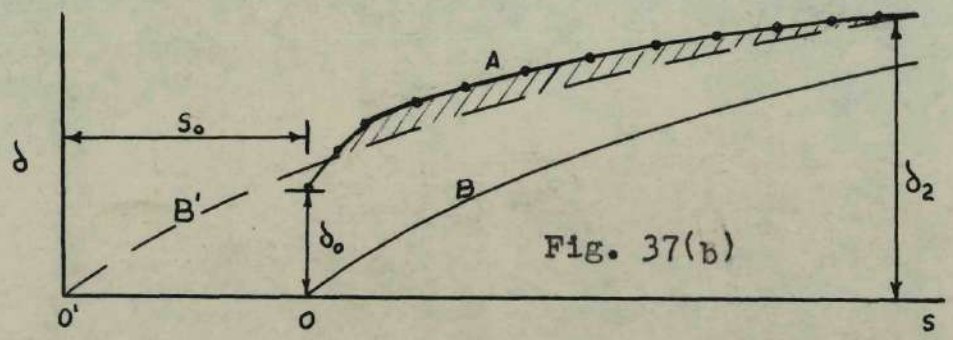

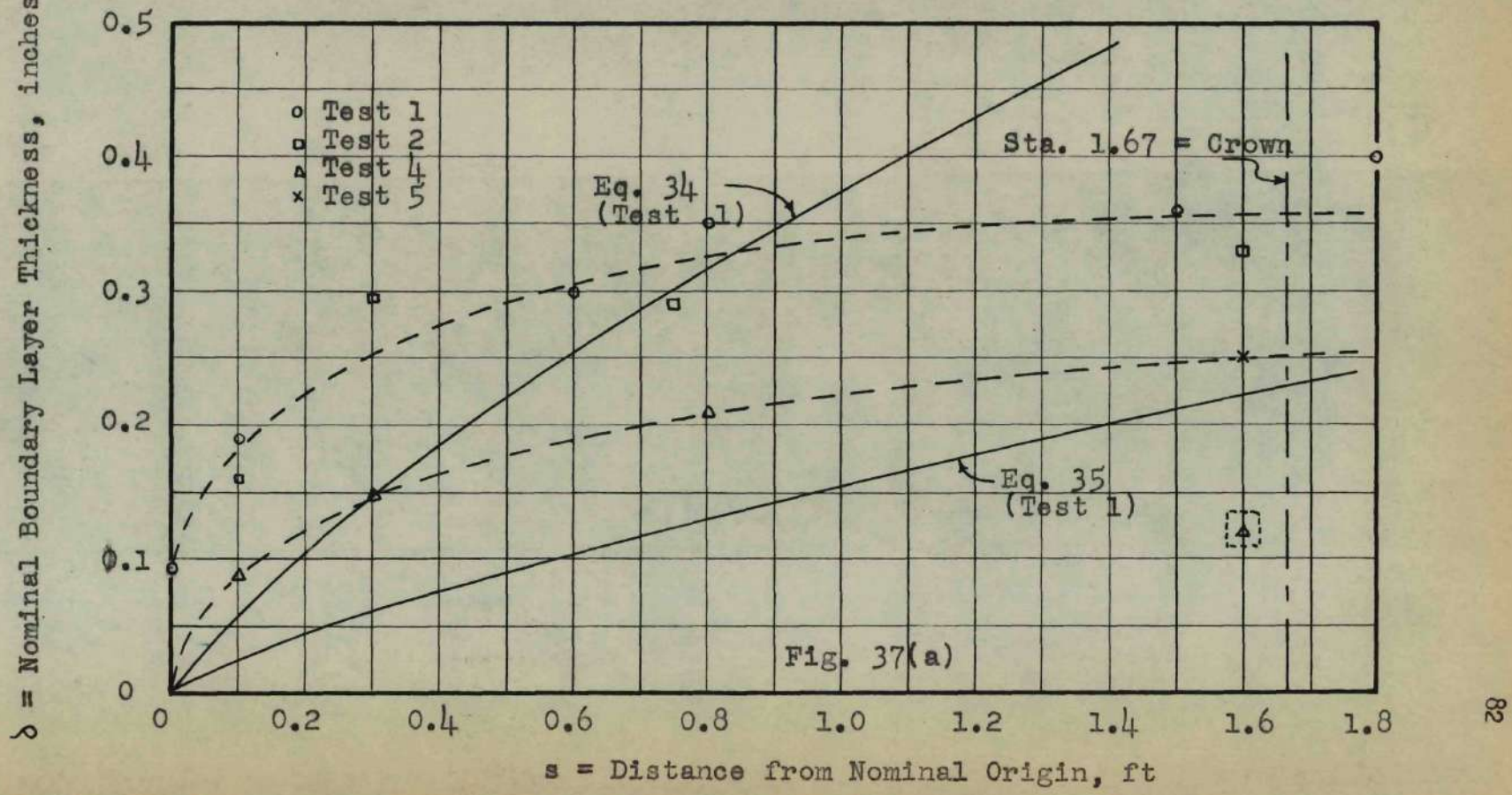

Fig. 37. GROWTH OF THE BOUNDARY LAYER.

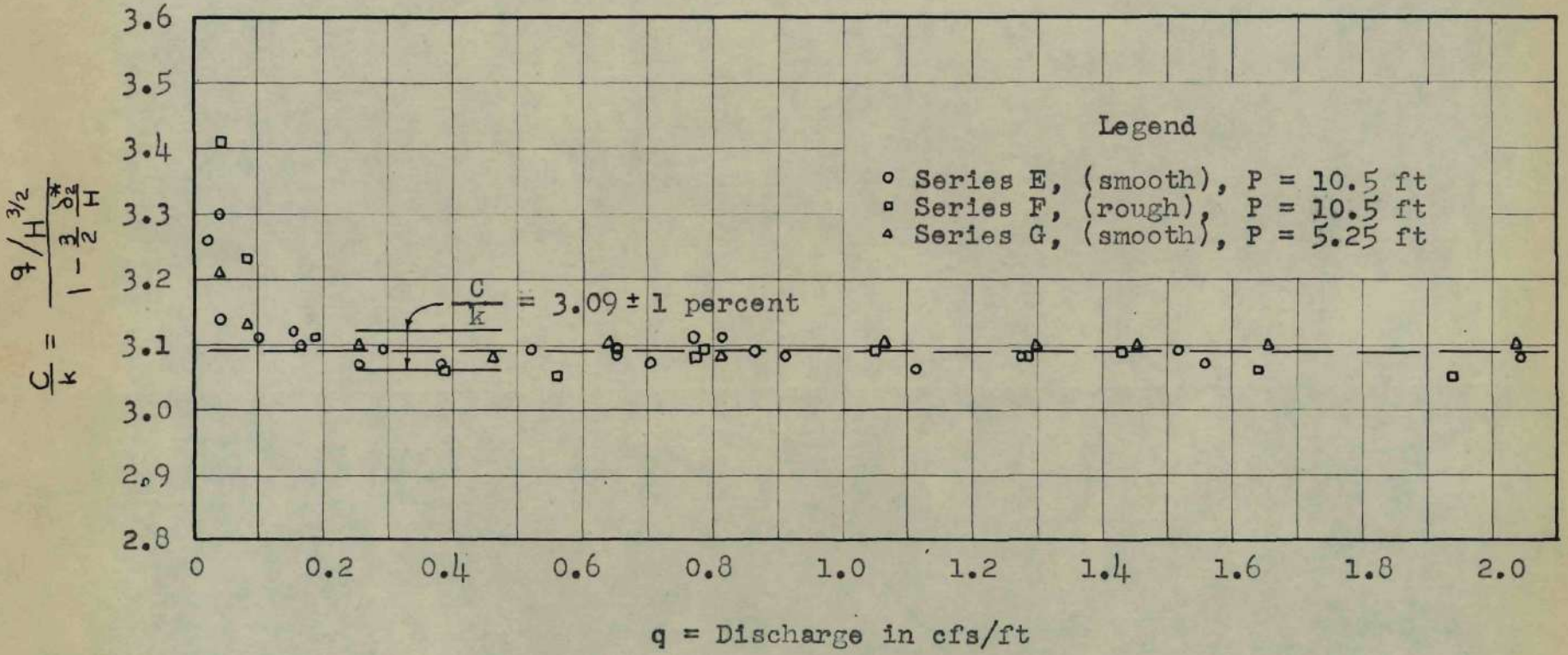

Fig. 38. VERIFICATION OF EQUATION 19.